1

The actin-modulating protein Synaptopodin mediates long-term survival of dendritic spines

4

Kenrick Yap[1], Alexander Drakew[1], Dinko Smilovic[1,2], Michael Rietsche[1], Mario Vuksic[1,2], Domenico Del Turco[1], Thomas Deller[1]

[1]Institute of Clinical Neuroanatomy
Dr. Senckenberg Anatomy
Neuroscience Center
Goethe University Frankfurt
Theodor-Stern-Kai 7
D-60590 Frankfurt/Main

[2]Croatian Institute for Brain Research
School of Medicine
University of Zagreb
Salata 12
10000 Zagreb, Croatia

Author for correspondence: Thomas Deller, M.D.
                                    email: t.deller@em.uni-frankfurt.de
                                    Tel.: +496963016900
                                    FAX: +496963016425

Keywords

29

Acknowledgement(s)

33 the memory of the late Michael Frotscher, M.D., who was a wonderful mentor and an enthusiastic

34 scientist and who was involved in many pioneering studies on the localization and the role of

35 Synaptopodin in the CNS.

36

40

41 **Competing interests / Conflict of Interest Statement**

42 The authors declare that the research was conducted in the absence of any commercial or financial

43 relationships that could be construed as a potential conflict of interest.

44

45 **Authors' contributions**

46 KY, DS, MR, MV acquired and analyzed data, AD analyzed and modeled data, DDT contributed tools,

47 TD conceived and supervised the study, TD, AD and KY wrote the manuscript with contributions from

48 all authors. All authors were involved in data interpretation and critically revising the manuscript. All

49 authors read and approved the final manuscript.

50   **Abstract**

51   Large spines are stable and important for memory trace formation. The majority of large spines also

52   contains Synaptopodin (SP), an actin-modulating and plasticity-related protein. Since SP stabilizes F-

53   actin, we speculated that the presence of SP within large spines could explain their long lifetime.

54   Indeed, using time-lapse 2-photon-imaging of SP-transgenic granule cells in mouse organotypic tissue

55   cultures we found that spines containing SP survived considerably longer than spines of equal size

56   without SP. Of note, SP-positive spines that underwent pruning first lost SP before disappearing.

57   Whereas the survival time courses of SP-positive (SP+) spines followed conditional two-phase decay

58   functions, SP-negative (SP-) spines and all spines of SP-deficient animals showed single exponential

59   decays. These results implicate SP as a major regulator of long-term spine stability: SP clusters stabilize

60   spines and the presence of SP indicates spines of high stability.

61   **Introduction**

62   Dendritic spines are protrusions found on the majority of excitatory neurons in vertebrate brains. They

63   form characteristic axo-spinous synapses and play an important role in integrating afferent synaptic

64   activity with postsynaptic activity (Yuste and Denk, 1995). The geometry of a spine, in particular, the

65   length of the spine neck and the size of the spine head are considered structural correlates of synapse

66   function: While the length of the spine neck has been linked to the biochemical and electrical isolation

67   of the spine compartment (Yuste et al., 2000; Yuste, 2013), the size of the spine head has been

68   positively correlated with AMPA-receptor density, synaptic strength and spine stability (Matsuzaki et

69   al., 2004; Kasai et al., 2010; McKinney, 2010). At the behavioral level, a critical role of spines in memory

70   formation and cognition has been discussed (Segal, 2005; Bourne and Harris, 2007; Kasai et al., 2010;

71   McKinney, 2010) and, indeed, a recent study has shown that spines are both necessary and sufficient

72   for memory storage and memory trace formation (Abdou et al., 2018).

73   The function of spines does not only depend on the shape and size of their outer membranes but also

74   on the molecular machinery within the spine subcompartment. A cellular organelle unique to spines is

75   the spine apparatus (Gray, 1959; Spacek, 1985), which consists of the stacked endoplasmic reticulum

76   (ER) and which modifies spine Ca^{2+} transients (Korkotian and Segal, 2011). Computational analyses

77   showed that the geometry of the spine apparatus in relation to the geometry of the surrounding spine

78   is a major determinant of second messenger dynamics (Cugno et al., 2018). Synaptopodin (SP) is an

79   essential component of the spine apparatus and mice lacking SP do not form the organelle and show

80   deficits in synaptic plasticity (Deller et al., 2003; Jedlicka et al., 2009; Vlachos et al., 2009; Vlachos et

81   al., 2013; Zhang et al., 2013; Korkotian et al., 2014; Jedlicka and Deller, 2017) as well as in spatial

82   learning (Deller et al., 2003).

83   The function of SP in spines is not limited to the formation of spine apparatus organelles. SP is also an

84   actin-modulating protein, which affects actin microfilaments either directly by stabilizing F-actin

4

85   (Mundel et al., 1997; Okubo-Suzuki et al., 2008) or indirectly via binding to alpha-actinin-2, Cdc42

86   ,RhoA or myosin V (Asanuma et al., 2005; Kremerskothen et al., 2005; Asanuma et al., 2006; Faul et

87   al., 2007; Jedlicka and Deller, 2017; Konietzny et al., 2019). Since spine geometry primarily depends on

88   actin assembly (Fischer et al., 1998; Matus, 2000; Konietzny et al., 2017), SP is likely to influence the

89   geometry and long-term stability of spines. Indeed, short-term imaging experiments performed in

90   dissociated cultures (Okubo-Suzuki et al., 2008; Vlachos et al., 2009) or acute slices (Zhang et al., 2013)

91   implicated SP in plasticity-induced spine head expansion. We have now expanded on these previous

92   studies and have used 2-photon time-lapse imaging of SP in granule cell spines to address the question

93   of whether SP is important for spine head size and long-term spine stability.

Materials and methods

94

Animals

95

96   Adult male mice (12-34 weeks) lacking SP (SP-KO, C57BL/6J background; (Deller et al., 2003), wild-type

97   mice (WT, C57BL/6J background) and Thy1-eGFP-SP x SP-KO mice (eGFP-SP-tg, C57BL/6J background

98   (Vlachos et al., 2013) were used for the ex vivo analysis of granule cell spines in fixed slices. eGFP-SP-

99   tg and SP-KO mice were used for the preparation of organotypic entorhino-hippocampal tissue

100   cultures. eGFP-SP-tg mice were obtained by crossing homozygote Thy1-eGFP-SP transgenic mice

101   (Vlachos et al., 2013) with SP-deficient mice (Deller et al., 2013). Thus, eGFP-SP-tg mice used for tissue

102   culture preparation were monoallelic for eGFP-SP and devoid of endogenous SP. Adult mice used for

103   fixed brain tissues were bred and housed at mfd Diagnostics GmbH, Wendelsheim, while mice used

104   for organotypic entorhino-hippocampal tissue cultures were bred and housed at the animal facility of

105   Goethe University Hospital Frankfurt. Animals were maintained on a 12 h light/dark cycle with food

106   and water available ad libitum. Experimental procedures and animal care were performed in

107   accordance with German animal welfare legislation and approved by the animal welfare officer of

108   Goethe University Frankfurt, Faculty of Medicine. Every effort was made to minimize the distress and

109   pain of animals.

110   Intracellular injections of granule cells in fixed tissue

111   After delivery, animals were kept in an in-house scantainer for a minimum of 24 h. Animals were killed

112   with an overdose of intraperitoneal Pentobarbital and subsequently intracardially perfused (0.1 M

113   Phosphate Buffer Saline (PBS) containing 4% paraformaldehyde (PFA)). Tail biopsies were obtained

114   after death to re-confirm the genotype. Brains were taken out immediately after perfusion, post-fixed

115   (18 h, 4% PFA in 0.1 M PBS, 4° C), washed trice in ice-cold 0.1 M PBS, sectioned (250μm) on a vibratome

116   (Leica VT 1000 S) and stored at 4 °C until use.

117 Intracellular injections of granule cells in fixed slices were performed as previously described

118 (Germroth et al., 1989; Hick et al., 2015), with modifications. Hippocampal slices were placed in a

119 custom-built, transparent and grounded recording chamber filled with ice-cold 0.1 M PBS. The

120 chamber was attached to an epifluorescent microscope (Olympus BX51WI; 10x objective

121 LMPlanFLN10x, NA 0.25, WD 21 mm) mounted on an x-y translation table (Science Products, VT-1 xy

122 Microscope Translator). Sharp quartz-glass microelectrodes (Sutter Instruments, QF100-70-10, with

123 filament) were pulled using a P-2000 laser puller (Sutter Instruments). Microelectrodes were tip-

124 loaded with 0.75mM Alexa568-Hydrazide (Invitrogen) in HPLC-grade water (VWR Chemicals, HiPerSolv

125 CHROMANORM) and subsequently back-filled with 0.1 M LiCl in HPLC-grade water. Microelectrodes

126 were attached to an electrophoretic setup via a silver wire and 500 MΩ resistance. The tip of the

127 microelectrode was navigated into the granule cell layer using a micromanipulator (Märzhäuser

128 Wetzlar, Manipulator DC-3K). A square-wave voltage (1mV, 1 Hz) was applied using a voltage generator

129 (Gwinstek SFG-2102). Granule cells were filled under visual control for at least 10 min or until no

130 further labeling was observed. Injected sections were fixed (4% PFA in PBS, overnight, 4 °C, in

131 darkness), washed in 0.1 M PBS and mounted on slides (Dako fluorescence mounting medium, Dako

132 North America Inc.). Only granule cells with dendrites reaching the hippocampal fissure were used for

133 analysis.

134 <u>Organotypic tissue cultures</u>

135 Organotypic entorhino-hippocampal tissue cultures (300 μm thick) were prepared from postnatal 4-5

136 days old eGFP-SP-tg mice of either sex as previously described with minor modifications (Del Turco and

137 Deller, 2007; Vlachos et al., 2012). Culture incubation medium contained 42% MEM, 25% Basal

138 Medium Eagle, 25% heat-inactivated normal horse serum, 25 mM HEPES, 0.15% sodium bicarbonate,

139 0.65% glucose, 0.1 mg/ml streptomycin, 100 U/ml penicillin, 2 mM glutamax, adjusted to pH 7.30. The

140 cultivation medium was refreshed every 2 to 3 days. All tissue cultures were allowed to mature in vitro

141 for at least 25 days in a humidified incubator (5% CO_2, at 35 °C).

142 <u>Laser microdissection</u>

143 Tissue cultures used for laser microdissection were washed with 0.1 M PBS, embedded in tissue-

144 freezing medium (Leica Microsystems) and shock-frozen (−80 °C) as previously described with minor

145 modifications (Vlachos et al., 2013). Sections (10 µm) were cut on a cryostat (Leica CM 3050 S) and

146 mounted on Poly Ethylene Terephthalate (PET) foil metal frames (Leicia Microsystems). Sections were

147 fixed in acetone (−20 °C, 30 sec), stained with 0.1% toluidine blue (Merck) at room temperature for 20

148 sec before rinsing in ultrapure water (DNase/RNase free, Invitrogen) and dehydrated in 70% (vol/vol)

149 and 100% ethanol. PET foil metal frames were mounted on a Leica LMD 6000 B system (Leica

150 Microsystems) and a pulsed UV laser beam was directed along the borders of the dentate granule cell

151 layer. Microdissected portions of the granule cell layer were collected in microcentrifuge tube caps

152 placed underneath the frame. Caps contained guanidine isothiocyanate-containing buffer (RNeasy

153 Mini Kit, Qiagen) and 1% β-mercaptoethanol (AppliChem GmbH). Microdissected tissue samples were

154 stored at −80 °C until further processing.

155 <u>RNA extraction and quantitative PCR</u>

156 Total RNA was isolated using the RNeasy Micro Plus Kit (Qiagen) and the purified RNA was reverse

157 transcribed into cDNA with a High Capacity cDNA Reverse Transcription Kit (Applied Biosystems)

158 following the manufacturers' instructions as previously described with minor modifications (Vlachos

159 et al., 2013). The cDNA was amplified using the StepOnePlus Real-Time PCR System (Applied

160 Biosystems) with a standard amplification protocol (14 cycles of 95 °C for 15 sec and 60 °C for 4 min),

161 and TaqMan PreAmp Master Mix Kit (Applied Biosystems) which contained 5 µL of PreAmp Master

162 Mix, 2.5 µL of cDNA and 2.5 µL of Assay Mix (TaqMan Gene Expression Assays from Applied Biosystems;

163 GAPDH, assay 4352932E; Synaptopodin, assay by design: forward primer, GTCTCCTCGAGCCAAGCA;

164 reverse primer, CACACCTGGGCCTCGAT; probe, TCTCCACCCGGAATGC). Amplified cDNAs were diluted

165 in ultrapure water (1:20) and quantitative PCR was performed using a standard amplification protocol

166 (1 cycle of 50 °C for 2 min, 1 cycle of 95 °C for 10 min, 40 cycles of 95 °C for 15 sec and 60 °C for 60 sec;

167 ending at 36 cycles).

168 Adeno-associated virus (AAV) production

169 HEK293T cells were transfected with pDP1rs (Plasmid Factory), pDG (Plasmid Factory), and tdTomato-

170 vector plasmid (12:8:5) by calcium phosphate seeding and precipitation (Grimm et al., 1998). Cells

171 were collected 48 h after transfection, washed twice with 0.1 M PBS, centrifuged at 1.500 x g for 5 min

172 and resuspended in 0.1 M PBS. Viral particles within the cells were released by 4 freeze-thaw cycles

173 and the supernatant centrifuged at 3,200 x g for 10 min to remove cell debris. The final supernatant

174 was collected, aliquoted and stored at -80 °C.

175 Viral labelling

176 To label dentate granule cells, tissue cultures were transduced with an AAV serotype 2 (AAV2)

177 containing the gene for tdTomato under the human Synapsin 1 promoter (Radic et al., 2017). Local

178 injections were performed on cultures using an injection pipette pulled from thin-walled borosilicate

179 capillaries (Harvard Apparatus, 30-0066). The pipettes were held by a head stage with a HL-U holder

180 (Axon Instruments) and positioned using a micro-manipulator (Luigs & Neumann). Approximately 0.05-

181 0.1 µl of AAV2-hSyn-tdTomato was injected directly into the suprapyramidal blade of the dentate gyrus

182 using a syringe. Tissue cultures were visualized with an upright microscope (Nikon FN1) equipped with

183 a camera and software (TrueChrome Metrics) using a 10x water immersion objective lens (Nikon Plan

184 Fluor, NA 0.30), which allowed precise injection of the AAV2 into the DG. Injections were performed

185 2-3 days after the tissue cultures were prepared.

186   Electron microscopy

187   Tissue cultures were fixed for 2 h in 0.1 M sodium cacodylate buffer (CB) containing 4% PFA, 4%

188   sucrose, 15% picric acid and 0.5% glutaraldehyde. After four washes in CB, the fixed cultures were

189   resliced to 40 μm. Following a wash with 0.1 M tris-buffered saline (TBS), free floating sections were

190   treated with 0.1% NaBH4 (Sigma-Aldrich) in TBS for 10 min to remove unbound aldehydes. Sections

191   were then blocked with 5% Bovine Serum Albumin (BSA) in TBS for 1 h at room temperature.

192   For detection of SP, sections were first incubated with rabbit anti-SP primary antibody (1:1000;

193   Synaptic Systems) in 2% BSA and 0.1 M TBS for 18 h at room temperature followed by incubation with

194   biotinylated goat anti-rabbit Immunoglobin G secondary antibody (1:200; Vector Laboratories,

195   Burlingame, CA) in 2% BSA and 0.1 M TBS for 75 min at room temperature. After three washes with

196   TBS, sections were incubated in avidin-biotin-peroxidase complex (ABC-Elite, Vector Laboratories) for

197   90 min at room temperature and treated with diaminobenzidine solution (Vector Laboratories) for 2-

198   15 min at room temperature. Sections were then incubated for silver-intensification in 3%

199   hexamethylenetetramine   (Sigma-Aldrich),   5%   silvernitrate   (AppliChem)   and   2.5%   di-

200   sodiumtetraborate (Sigma-Aldrich) for 10 min at 60 °C, followed by 0.05% tetrachlorogold solution

201   (AppliChem) for 3 min and 2.5% sodium thiosulfate (Sigma-Aldrich) for 3 min with three washes after

202   each step using distilled water.

203   After immunostaining, sections were washed in 0.1 M CB, treated with 0.5% OsO4 (Plano) in 0.1 M CB

204   for 30 min, dehydrated in increasing concentrations of ethanol and then 1% uranyl acetate (Serva) in

205   70% ethanol for 60 min, before being embedded in Durcupan (Sigma Aldrich) for ultrathin sectioning

206   (60 nm thickness). Sections were collected on single slot Formvar-coated copper grids and investigated

207   using an electron microscope (Zeiss EM 900).

208   Confocal microscopy of fixed hippocampal slices

209   Confocal imaging of fixed dendritic segments from identified, Alexa568-labeled dentate granule cells

210   in the outer molecular layer (OML) of the suprapyramidal blade was done with an Olympus FV1000

211   microscope and a 60x oil-immersion objective (UPlanSApo, NA 1.35, Olympus) using FV10-ASW

212   software with 5x scan zoom at a resolution of 1024 x 1024 pixels. To ensure localization in the OML,

213   3D image stacks of dendritic segments (0.25 μm z-axis step size) were taken at a distance of 10-50 μm

214   from the hippocampal fissure. Crossing dendritic segments or branch points were avoided to facilitate

215   spine attribution to a given segment.

216   2-Photon time-lapse imaging of tissue cultures

217   Live imaging of tdTomato-labelled granule cells with eGFP-tagged SP clusters was done using an

218   upright 2-photon microscope (Scientifica MPSLSC-1000P, East Sussex, UK) equipped with a 40x water

219   immersion objective (Zeiss Plan-Apochromat, NA 1.0) and a Ti-sapphire mode-locked laser (MaiTai,

220   Spectra-Physics) tuned to a wavelength of 1000 nm to excite both eGFP and tdTomato. The membrane

221   insert containing the cultures was placed in a petri dish containing warm imaging buffer consisting of

222   129 mM NaCl, 4 mM KCl, 1 mM MgCl2, 2 mM CaCl2, 4.2 mM glucose, 10 mM HEPES buffer solution,

223   0.1 mM Trolox, 0.1 mg/ml streptomycin, 100 U/ml penicillin, and pH 7.4. 3D image stacks of dendritic

224   segments (~50-80 μm in length) located in the middle to outer molecular layers (15-25 images per

225   stack, 0.5 μm z-axis step size) were acquired using ScanImage 5.1 (Pologruto et al., 2003) with 8x digital

226   zoom at a resolution of 512 x 512 pixels, i.e. 0.07 μm x 0.07 μm in the focal plane. The same dendritic

227   segments across imaging sessions were identified using nearby landmarks and neighboring dendrites.

228   Imaging time was minimized (only 1 dendritic segment per culture was imaged) to minimize the risk of

229   phototoxic damage.

230   Image processing and data analysis

231   The images obtained were deconvolved with Huygens Professional Version 17.10 (Scientific Volume

232   Imaging, The Netherlands, http://svi.nl). Image processing and data analysis were then performed

233   using Fiji version 1.52h (Schindelin et al., 2012), with spine analysis adapted from published criteria

234   (Holtmaat et al., 2009).

235   Dendritic spines of all shapes were assessed manually on z-stacks of dendritic segments in the middle

236   to outer molecular layers. Only protrusions emanating laterally in the x-y directions, not above or

237   below the dendrite, and exceeding the dendrite for at least 5 pixels (0.35 μm; 0.2 μm for confocal)

238   were included for analysis (Holtmaat et al., 2009; Vlachos et al., 2012).

239   For spine head size and SP cluster size measurements, the maximum cross-sectional area of the spine

240   head or SP cluster in one of the x-y planes within the z-stack was measured. A spine was considered

241   SP+ if the SP cluster overlapped with the spine head and/or neck in both the x-z and y-z directions

242   when scrolling through the z-stacks. For spine stability analysis, we examined ~15 μm long

243   subsegments exhibiting minimal dendritic distortion over the total observation period. Individual

244   spines were re-identified at consecutive points in time based on their relative positions to nearby

245   landmarks and neighboring spines (Holtmaat et al., 2009; Vlachos et al., 2012). The presence or

246   absence of a particular spine at a certain time point was verified by scrolling through the z-stacks to

247   avoid misclassification due to rotation of the dendritic segment.

248   Spine turnover ratio representing the fraction of all observed spines that appear and/or disappear

249   during the total imaging period was measured (adapted from Holtmaat, et al., 2009). Spine turnover

250   ratio = (Ngained + Nlost) / (2 x Ntotal), where Ngained is the number of spines gained between the

251   initial observation time point of t = -1 and the final observation time point of t = 12, Nlost is the number

252   of spines lost between t = -1 and t = 12, and Ntotal is the total number of spines that were observed

253   at one or more points in time. Spine formation ratio = (Ntotal – Ninitial) / (Ntotal), where Ninitial is the

254   number of spines observed at t = -1. Spine loss ratio = (Ntotal – Nfinal) / (Ntotal), where Nfinal is the

255   number of spines observed at t = 12.

256   <u>Statistical analysis</u>

257   Statistical tests and n-values are indicated in figure captions. Statistical tests were chosen based on the

258   experimental conditions, i.e. (1) matched-pairs, (2) two independent groups, (3) multiple matched-

259   pairs, or (4) multiple independent groups. Thus, statistical comparisons were performed using

260   Wilcoxon signed rank test with Pratts modification accounting for ties and zero differences in case of

261   comparing integer values (differences between matched pairs under the null hypothesis of no

262   difference), Mann-Whitney U-test (comparing two independent groups), Friedman test (for

263   differences between matched pairs of multiple groups), and Kruskal-Wallis test (comparing multiple

264   groups). Dunn's multiple comparison test was applied following one of the two latter tests in case of

265   significant P-values. All statistical tests were performed using GraphPad Prism 6. If P values were less

266   than 0.05 the null-hypothesis was rejected. Statistical values were expressed as mean ± standard error

267   of mean (SEM), unless otherwise stated. $*p < 0.05$, $**p < 0.01$, $***p < 0.001$.

268   <u>Modeling of spine survival and loss</u>

269   The fractions of surviving spines observed at distinct time points were fitted to different models of

270   spine survival and loss, respectively (see results). Curve fitting was performed with the user-defined

271   fitting function of GraphPad Prism 6. Decay functions were fitted to the data weighted by $1/Y^2$ using

272   least squares fit. The resulting spine loss curves correspond to the probability that single spines

273   experience a particular survival time. Therefore, the loss curves represent the cumulative density

274   function of spine survival times. We derived the distribution of spine survival times underlying the

275   spine loss curves from the inverse loss curves. Since there is no analytical solution for the inverse of

276 the conditional two stage decay, the inverse loss functions (i.e. the inverse cumulative density

277 functions of spine survival times) were obtained from the spine loss models numerically as follows:

278 According to the diverse loss models, the fractional survival was calculated for 10^7 equally spaced time

279 points ranging from zero to 30 times the longest time constant of the respective decay function. For

280 each of 10^5 equally spaced bins of fractional survival, the mean of the corresponding times (X-axis) was

281 defined as the survival time corresponding to 1 minus the center of the respective fractional survival

282 interval. The distribution of survival times displayed in the figures was derived as the histogram of

283 these values using a bin size of 100. The median as well as the 10th, 25th, 75th, and 90th percentile of

284 these distributions are also displayed in the figures. Statistical comparisons of median survival times

285 between groups were based on the medians of 10 random samples of sizes equal to the number of

286 observed spines per group using the Mann-Whitney U-Test. Derivation of survival times was

287 performed using LabVIEW 2019 (National Instruments).

288   **Results**

289   Synaptopodin is present in large granule cell spines in vivo

290   Previous work reported a positive correlation between the plasticity-related protein SP and spine head

291   size (Okubo-Suzuki et al., 2003; Vlachos et al., 2009; Zhang et al., 2013). Since SP-deficient mice show

292   deficits in synaptic plasticity (Deller et al., 2003; Jedlicka 2009; Zhang et al., 2013; Grigoryan and Segal,

293   2016), we speculated that SP-deficient neurons might have smaller spine head sizes, providing a

294   structural explanation for the plasticity phenotype. Accordingly, we analyzed and compared spine head

295   size in hippocampal tissue sections of wildtype and SP-deficient mice (Deller et al., 2003) bred on the

296   C57BL/6J genetic background. Surprisingly, Alexa 586-filled wildtype and mutant granule cells (Fig. 1A,

297   B) showed similar average spine head sizes (Fig. 1C) and spine head size distributions (Fig. 1D). Next,

298   we re-visited the relationship between SP and spine head size that had been suggested earlier (Okubo-

299   Suzuki et al., 2003; Vlachos et al., 2009; Zhang et al., 2013). Using Alexa 568-injected granule cells from

300   eGFP-SP-tg mouse brain (Fig. 1E; Vlachos et al., 2013), we first studied the fraction of SP-positive spines

301   and found SP clusters in ~14% of spines (Fig. 1F). Spines containing SP (SP+) were significantly larger

302   than spines without SP (SP-) (Fig. 1G) and showed a right shifted cumulative frequency distribution

303   (Fig. 1H). In addition, SP cluster size was positively correlated with spine head size (Fig. 1I),

304   demonstrating that large SP clusters are typically found in large spines. We conclude from these in vivo

305   observations that SP is indeed tightly correlated with spine size. However, SP does not appear to be a

306   major regulator of spine head size, since neither average spine head size nor spine head size

307   distributions were affected by SP-deficiency (Fig. 1D).

308   This surprising finding raised the question of what is the role of SP in large spines, if SP is not a regulator

309   of head size? Since SP is an actin-modulating plasticity-related protein, it has been speculated that SP

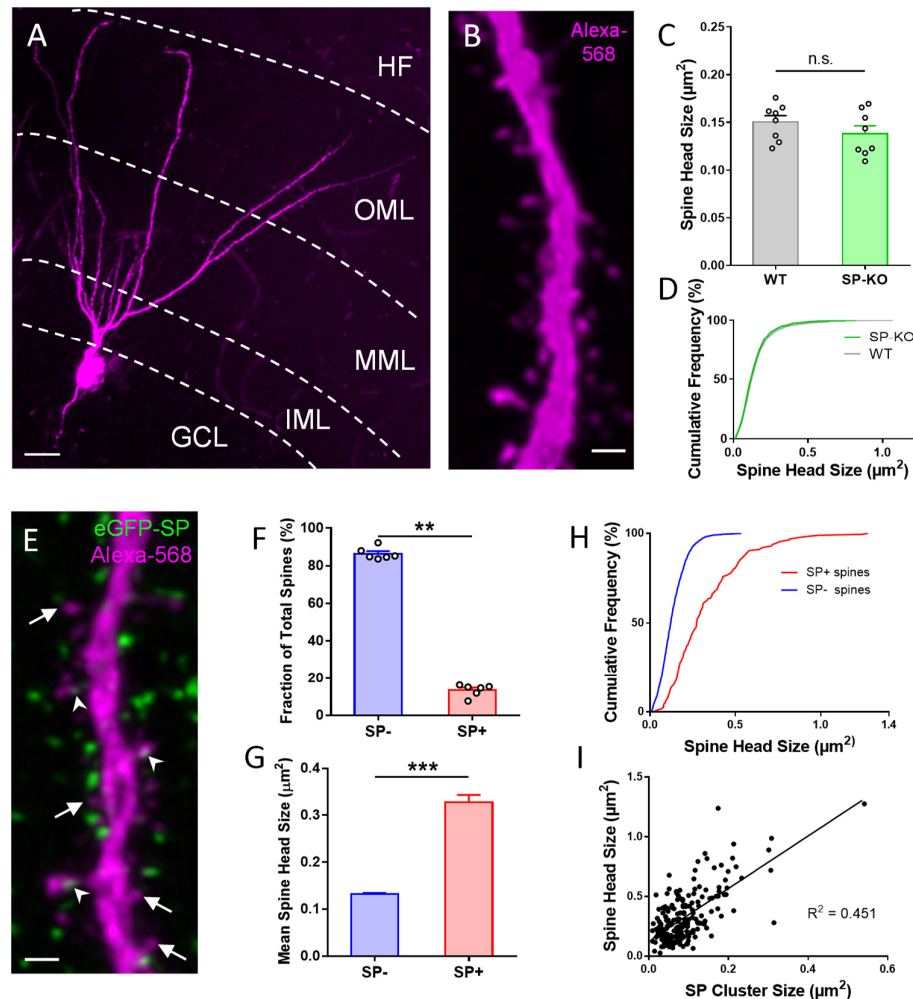310   could also regulate spine stability (e.g. Deller et al., 2000).

Figure 1. SP is associated with large granule cell spines in adult mouse dentate gyrus. (A) Granule cell located in the suprapyramidal blade of the dentate gyrus of a SP-knock-out (SP-KO) mouse intracellularly filled with the fluorescent dye Alexa-568 (magenta; fixed tissue). Dendritic segments in the outer molecular layer (OML) were used for analysis. MML: middle molecular layer. IML: inner molecular layer. GCL: granule cell layer. HF: hippocampal fissure. Scale bar = 20 μm. (B) Dendritic segment of a SP-KO granule cell shown at higher magnification. Scale bar = 1 μm. (C) Spine head sizes of wildtype (WT) and SP-KO mice. n.s., not significant; $p = 0.291$, Mann-Whitney U-test. WT mice and SP-KO mice, n = 8 per group (3 dendritic segments per animal; 1885 WT spines, 2158 SP-KO spines). (D) Cumulative frequency plots of spine head sizes of wildtype (grey) and SP-KO (green) mice. (E) Granule cell located in the suprapyramidal blade of the dentate gyrus of a Thy1-eGFP-SP-transgenic mouse bred on a SP-KO background (eGFP-SP-tg mouse) intracellularly filled with Alexa-568 (magenta; fixed tissue; OML). Arrowheads point to eGFP-SP clusters (green) in SP-positive (SP+) dendritic spines. Arrows mark SP-negative (SP-) spines. Scale bar = 1 μm. (F) Fractions of SP- (~86.5%) and SP+ (~13.5%) spines. **$p < 0.0022$, Mann-Whitney U-test. eGFP-SP-tg mice, n = 6. (G) Mean spine head size of SP- (~0.133 μm^2) and SP+ (~0.328 μm^2) spines. ***$p < 0.0001$, Mann-Whitney U-test. SP+ spines n = 200; SP- spines n = 1497. (H) Cumulative frequency plots of spine head sizes of SP- (blue) and SP+ (red) spines. SP+ spines = 200; SP- spines = 1497. (I) Correlation analysis of spine head size and SP cluster size: Spearman coefficient of correlation = 0.536, 95% C.I.: 0.426 – 0.630. ***$p < 0.0001$. Linear regression analysis: $R^2 = 0.451$. n = 200 spines.

16

329   As previous reports have shown that large cortical spines are more stable than small spines (Kasai et

330   al., 2003; Matsuzaki et al., 2004; Bourne and Harris, 2008; Kasai et al., 2010; McKinney, 2010), we

331   speculated that the presence of SP in these spines could explain or at least contribute to their higher

332   stability. To test this hypothesis, we used an organotypic tissue culture preparation, which allowed us

333   to follow not only spine geometry – which can also be done in vivo – but also the dynamics of SP

334   clusters within spines over time.

335   <u>Synaptopodin is present in large granule cell spines in organotypic tissue cultures</u>

336   Organotypic tissue cultures of the entorhinal cortex and hippocampus were generated from eGFP-SP-

337   tg mice. In these cultures SP clusters were abundant in the molecular layer of the dentate gyrus (Fig.

338   2A), similar to what has been described for wildtype animals after SP immunolabeling (Deller et al.,

339   2000b; Bas Orth et al., 2005). To visualize single granule cells and their spines, tissue cultures were

340   virally transduced on 2-3 DIV using an AAV2-tdTomato virus. After approximately three weeks in vitro,

341   tdTomato expressing granule cells were imaged and spines with SP (SP+) and without SP (SP-; Fig. 2B)

342   were identified. SP+ spines also contained SP-positive spine apparatus organelles (Fig. 2C). SP mRNA

343   expression levels in eGFP-SP-tg cultures were similar to SP mRNA expression levels in granule cells of

344   SP +/+ wildtype cultures (Fig. 2D). Since SP had been suggested to regulate spine head size (see

345   previous paragraph), we also investigated average spine head size and spine head size distribution in

346   SP-deficient cultures (Fig. 2E, F). No significant differences between SP-deficient and eGFP-SP-tg

347   granule cells were seen, in line with our in vivo observations (c.f. Fig. 1), suggesting again that SP is not

348   a major regulator of spine head size.

349   Next, we analyzed the fraction of SP+ and SP- spines and found that approximately 8% of all granule

350   cell spines are SP+ (Fig. 2G). Analysis of head sizes of SP+ and SP- spines (Fig. 2; Suppl. Fig 1 related to

351   Fig. 2) revealed that SP+ spines are on average much larger than SP- spines (SP- spines: 0.364 ± 0.005

352   μm^2; SP+ spines: 0.801 ± 0.029 μm^2; Fig. 2H), similar to what was observed in vivo (c.f. Fig. 1).
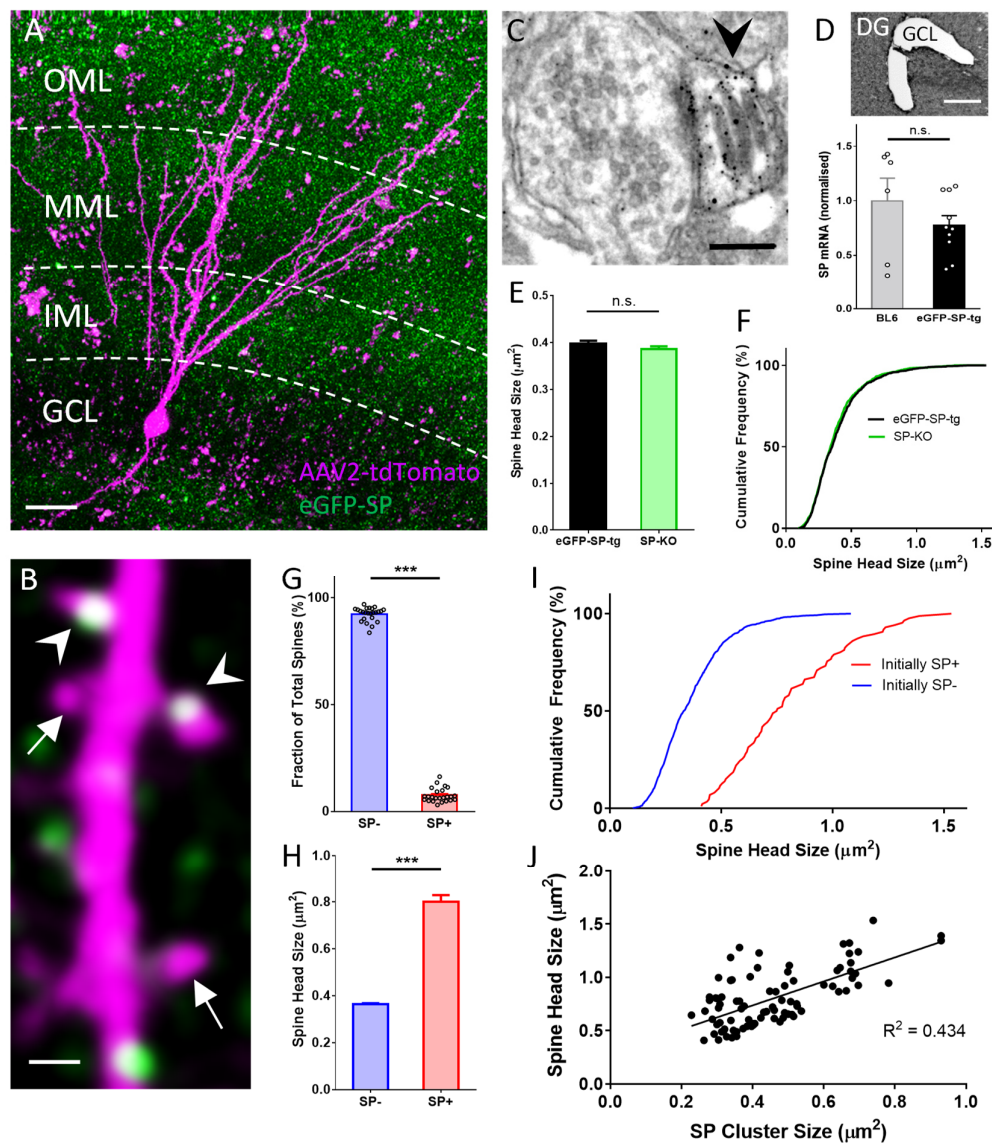
353

Figure 2. SP in dendritic spines of granule cells in organotypic tissue cultures of hippocampus. (A) Granule cells in organotypic entorhino-hippocampal tissue cultures (OTCs) of eGFP-SP-tg (green) mice were virally transduced (AAV2) with tdTomato (magenta) at day in vitro (DIV) 2-3. Dendritic segments located in the middle molecular layer (MML) or in the outer molecular layer (OML) were imaged. GCL, granule cell layer; IML, inner molecular layer. Scale bar = 20 μm. (B) Single plane 2-photon image of a granule cell dendrite in the OML. Arrowheads point to SP+ spines; arrows indicate SP- spines. Scale bar = 1 μm. (C) Electron micrograph of a SP+ spine (arrowhead) containing an immunolabeled spine apparatus in an OTC from an eGFP-SP-tg mouse. Scale bar = 0.2 μm. (D) SP-mRNA levels in microdissected granule cell layers (GCL; upper panel) from OTCs of eGFP-SP-tg and C57BL/6J (BL6) wildtype mice were not significantly different (lower panel). p = 0.353, Mann-Whitney U-test. Number of BL6 tissue cultures n = 6; number of eGFP-SP-tg tissue cultures n = 10. DG, dentate gyrus. Scale bar = 100 μm. (E) Mean spine head sizes of eGFP-SP-tg (black) and SP-KO (green) granule cells. n.s., not significant. p = 0.211, Mann-Whitney U-test. Number of spines: eGFP-SP-tg n = 1107; SP-KO n = 1113, obtained from 24 segments, 1 segment per culture. (F) Cumulative frequency plots showing the distribution of spine head sizes of these spines. (G) SP+

367 spines comprised 7.6% of the total spine population. ***p < 0.0001, Mann-Whitney U-test. Percentage per eGFP-
368 SP-tg dendritic segment; n = 24 segments. (H) SP+ spines were significantly larger than SP- spines. ***p < 0.0001,
369 Mann-Whitney U-test. Number of SP+ spines n = 87, SP- spines n = 1021. (I) Cumulative frequency plots showing
370 the distribution of spine head sizes of SP+ and SP- spines. (J) SP cluster size and spine head size of SP+ spines are
371 tightly correlated: Spearman coefficient of correlation = 0.565, 95% C.I.: 0.396 – 0.697. ***p < 0.0001. Linear
372 regression analysis: R^2 = 0.434. n = 87 spines.

373

374 The following figure supplements are available for Figure 2.
375 **Figure S1 related to Figure 2. Measurement of dendritic spine head size and SP cluster size.**

376

377 Likewise, cumulative frequency diagrams showed that the population of SP+ spines is right-shifted

378 towards larger spine head sizes compared to SP- spines (Fig. 2I). Finally, correlation analysis of SP

379 cluster size and spine head size demonstrated a positive correlation between the two parameters (Fig.

380 2J). We conclude from these observations that with regard to SP granule cells in organotypic tissue

381 cultures are highly similar to granule cells in vivo (c.f. Fig. 1). Furthermore, we conclude that SP is

382 preferentially found in large granule cell spines.

383 <u>Presence and size of Synaptopodin clusters in vitro are tightly associated with bidirectional changes in</u>

384 <u>spine head size</u>

385 After demonstrating significant differences in average spine head size between SP+ and SP- spines, we

386 wondered whether this relationship between SP and spine head sizes is also seen under dynamic

387 conditions, i.e. when spines undergo changes in their head size. For this, we studied how insertion and

388 loss of SP clusters from spines affects spine head geometry (Fig. 3). Single spines containing SP and

389 spines devoid of SP were identified and spine head sizes were measured on two consecutive days (Fig.

390 3). Four groups of spines were distinguished: Spines gaining SP (Fig. 3A), spines losing SP (Fig. 3B),

391 spines maintaining SP (Fig. 3C), and spines remaining SP- (Fig. 3D). This analysis revealed a robust

392 correlation between increases in spine head size and insertion of SP and decreases of spine head size
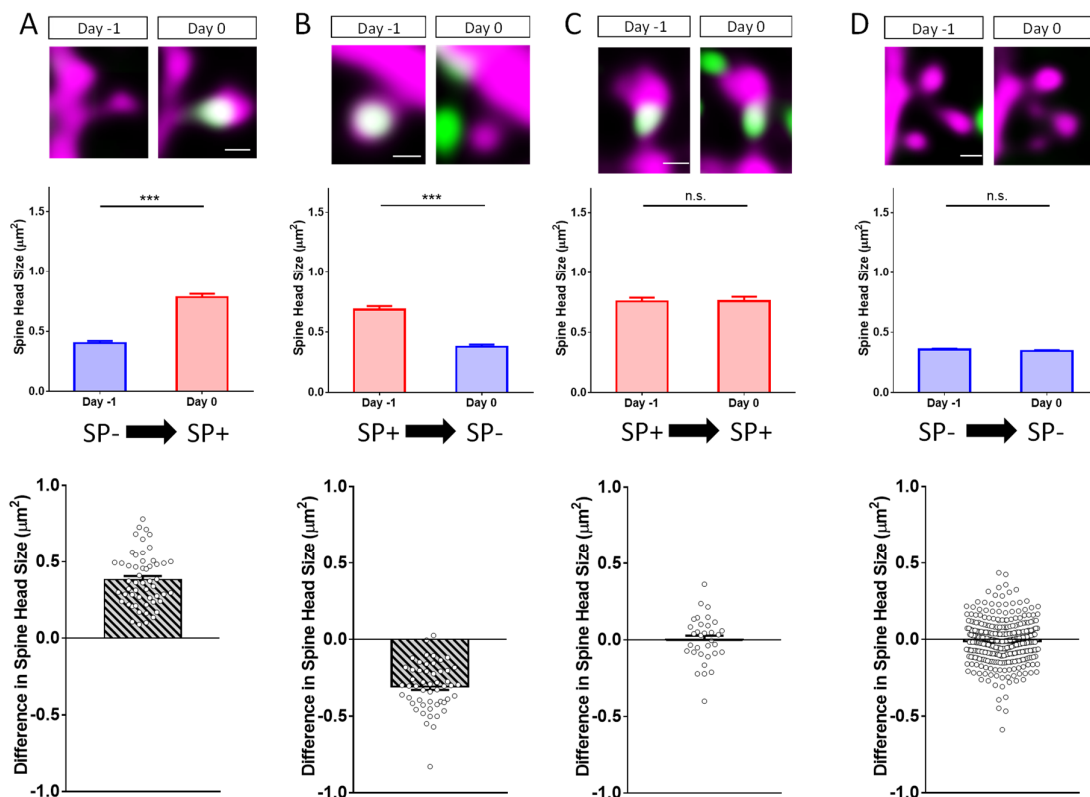
393 and loss of SP from spines (Fig. 3).

Figure 3. Changes in spine SP content are associated with bidirectional changes in spine head size. Sample spines (upper panels), mean spine head size changes (middle panels) and differences in spine head size of individual spines (lower panels) are illustrated. (A) Example of a spine that became SP+ between day -1 and 0. The mean maximum cross-sectional spine head area of spines of this group increased significantly. ***p < 0.0001, Wilcoxon matched-pairs signed rank test. Number of spines n = 54. Scale bar = 0.5 µm. (B) Example of a spine that was SP+ and became SP- between day -1 and 0. The mean maximum cross-sectional spine head area of spines of this group decreased significantly. ***p < 0.0001, Wilcoxon matched-pairs signed rank test. Number of spines n = 52. Scale bar = 0.5 µm. (C) Example of a spine that remained SP+. The mean cross-sectional spine head area of spines of this group did not change significantly. p = 0.850, Wilcoxon matched-pairs signed rank test. Number of spines n = 33. Scale bar = 0.5 µm. (D) Example of a spine that remained SP-. The mean cross-sectional spine head area of spines of this group did not change significantly. p = 0.060, Wilcoxon matched-pairs signed rank test. Number of spines n = 340. Scale bar = 0.5 µm.

The presence of Synaptopodin in spines is associated with long-term spine survival

The stability of spines is important for maintaining specific connections between neurons. Since SP

stabilizes F-actin (Okubo-Suzuki et al., 2008), we speculated that SP could have an effect on long-term

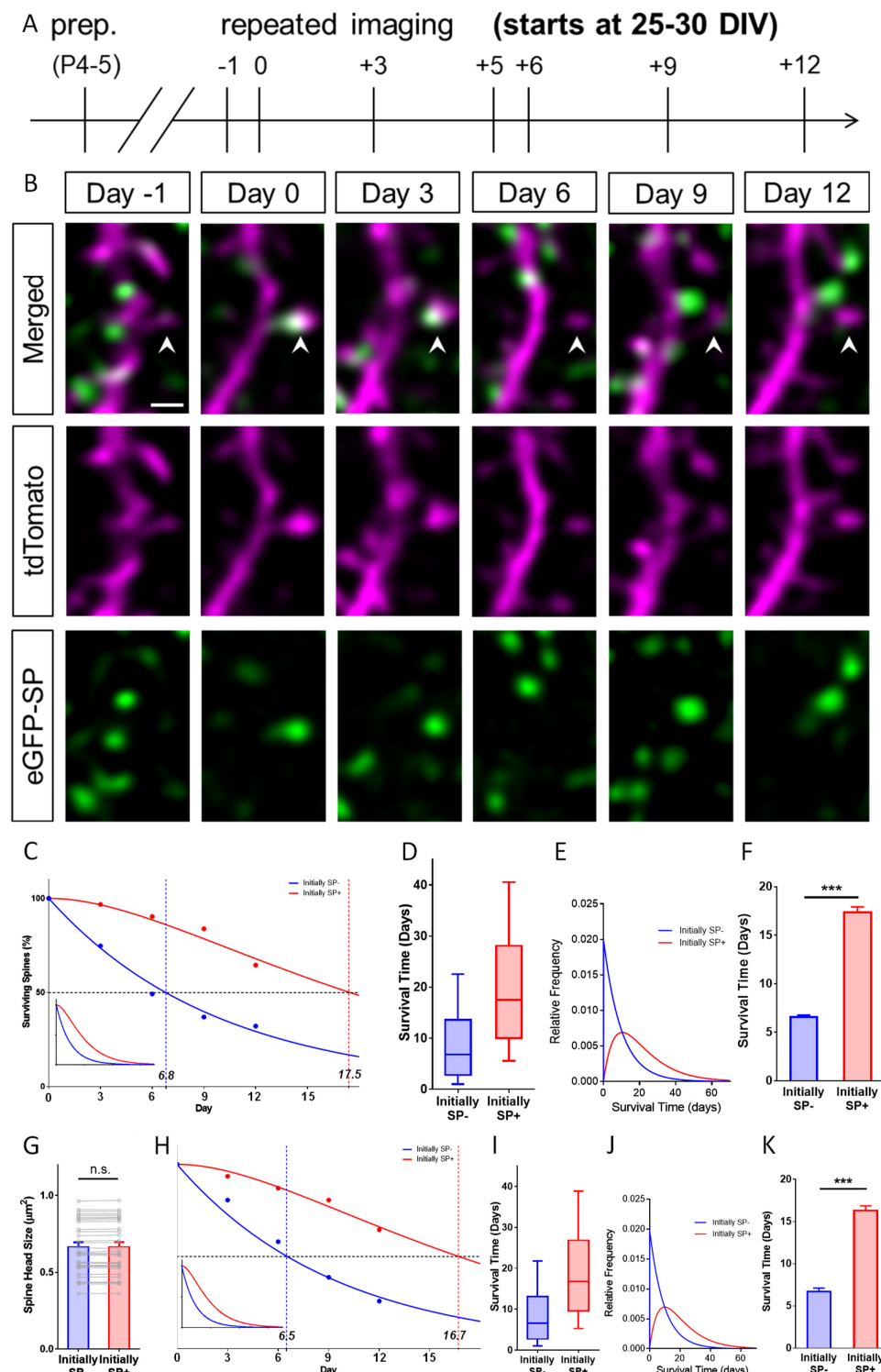spine stability (Deller et al., 2000a; Jedlicka and Deller, 2017).

Figure 4. SP+ spines are highly stable spines. (A) Schematic of the experimental design. OTCs were prepared at postnatal day (p) 4-5 from eGFP-SP-tg mice and allowed to mature for 25-30 DIV. Time-lapse 2-photon imaging

415   of identified dendritic segments was performed at time points as indicated. (B) Time-lapse imaging of a granule

416   cell dendrite over 14 days illustrates the dynamics of SP clusters within individual spines. Arrowhead points to a

417   spine that became SP+ on day 0, stayed positive on day 3, lost SP between days 3 and 6 and then remained SP-

418   until day 12. Scale bar = 1 μm. (C) The survival of SP+ (red curve) and SP- spines (blue curve) was studied from

419   day 0 until day 12. Dots: observed fractions; curves: fitted to observation points. The median survival of initially

420   SP- spines was ≈ 6.8 days whereas the median survival of initially SP+ spines was ≈ 17.5 days. Number of spines

421   at day 0: SP+ = 31, SP- = 392. Inset: Calculated decay curves until day 70. SP- spines followed a single stage decay

422   function whereas SP+ spines followed a conditional two stage decay function. (D) Survival times of the total

423   populations of SP+ and SP- spines derived from the fitted survival curves. Boxes indicate median, lower and upper

424   quartiles. Whiskers indicate 10th and 90th percentiles, respectively. (E) Relative frequency distributions of these

425   survival times. (F) The survival time of SP+ spines was significantly longer than SP- spines; computational model;

426   ***p < 0.0001, Mann-Whitney U-test; based on 10 samples of 31 SP+ and 392 SP- spines. (G) To control for

427   differences in spine head size, SP+ and SP- spines of equal head size were matched. The spine head size of these

428   pairs was not significantly different. p = 0.310, Wilcoxon matched-pairs signed rank test. Number of size-matched

429   pairs n = 31. (H) The decay curve of these size-matched spines was very similar to the decay curve of all SP+ and

430   SP- spines. The median survival of SP- spines of this population was ≈ 6.5 days, whereas size-matched SP+ spines

431   showed a median survival of ≈ 16.7 days. Inset: Calculated decay curves until day 70. (I) Survival times of the total

432   populations of SP+ and SP- spines derived from the fitted survival curves. (J) Relative frequency distributions of

433   these survival times. (K) The survival time of size-matched SP+ spines was significantly higher than that of SP-

434   spines; computational model; ***p < 0.0001, Mann-Whitney U-test. based on 10 samples of 31 SP+ and 31 SP-

435   spines.

436

437   To address this hypothesis, we used time-lapse imaging and followed single spines for two weeks (Fig.

438   4A). During this time period, we determined their SP content, head sizes and fate (Fig. 4A, B). This

439   analysis revealed major differences in the survival time of SP+ and SP- spines (Fig. 4C-E): Whereas the

440   median survival time of SP+ spines was ~17.5 days, the median survival time of SP- spines was only

441   ~6.8 days (Fig. 4C).

442   In addition to this notable difference in median survival time, the curves that fitted our data turned

443   out to be fundamentally different: Whereas SP- spines followed a single phase exponential decay

444   function, the decay of SP+ spines could only be fitted using a conditional double phase exponential

445   decay function (see below; Fig. 4C). Based on these two functions the distributions of long-term

446   survival times (Fig. 4D, E) of the SP- and SP+ spine populations were calculated (see methods). Finally,

447   a data-driven simulation of spine survival was performed to test whether the survival times of the two

448   spine populations are different. This approach revealed – within the parameters used – that SP- and

449   SP+ spines differ significantly in their survival times (Fig. 4F).

450   Since SP+ spines are larger than SP- spines (c.f. Fig. 1G, 2H) the observed effect on spine survival could

451   simply be the result of differences in head size between the two groups. As large spines have been

452   shown to be more stable (Kasai et al., 2003; Matsuzaki et al., 2004; Bourne and Harris, 2008; Kasai et

453   al., 2010; McKinney, 2010), this would be a straightforward explanation. We controlled for this

454   possibility by comparing the survival times of SP+ and SP- spines of equal head size (matched pairs; Fig.

455   4G). Even under these highly constrained conditions the difference in spine survival between SP+ and

456   SP- spines was still observed (Fig. 4H). In line with this, the overall distributions (Fig. 4I), the relative

457   frequency distributions of spine survival times of the calculated total populations of spines (Fig. 4J), as

458   well as simulations of spine survival (Fig. 4K) were comparable to those found for all spines, i.e. non-

459   size-matched spines.

460   <u>Synaptopodin increases survival of small, medium and large spines</u>

461   Since the stability of large spines is higher than the stability of small spines (Kasai et al., 2003; Matsuzaki

462   et al., 2004; Bourne and Harris, 2008; Kasai et al., 2010; McKinney, 2010), we wondered whether this

463   difference could be caused by the presence of SP within large spines. This appeared to be a possibility

464   since SP is tightly associated with the population of large and stable spines and rare in the group of

465   small and less stable spines (Fig. 5A, B). Should the increased stability of large spines depend on SP we

466   made two testable predictions: (1) If SP is present in small spines, it should increase survival of these

467   spines irrespective of their size, and, (2) if SP is absent from large spines, these spines should be pruned

468   faster in spite of their large size. To test these hypotheses, we subdivided SP+ and SP- spines into four

469   size classes (Fig 5B; very small, small, medium and large spines) and compared the survival times of SP-

470   and SP+ spines belonging to each of these classes. To test the first hypothesis, we analyzed the three

471   smaller size groups, which comprise the majority (~95%) of all spines (Fig. 6A). SP was completely

23

472   absent from the very small spine group, in which ~41% of all SP- spines are found (Fig. 5B). This spine

473   population rapidly decayed with time following a single exponential decay function (Fig. 5C-F).
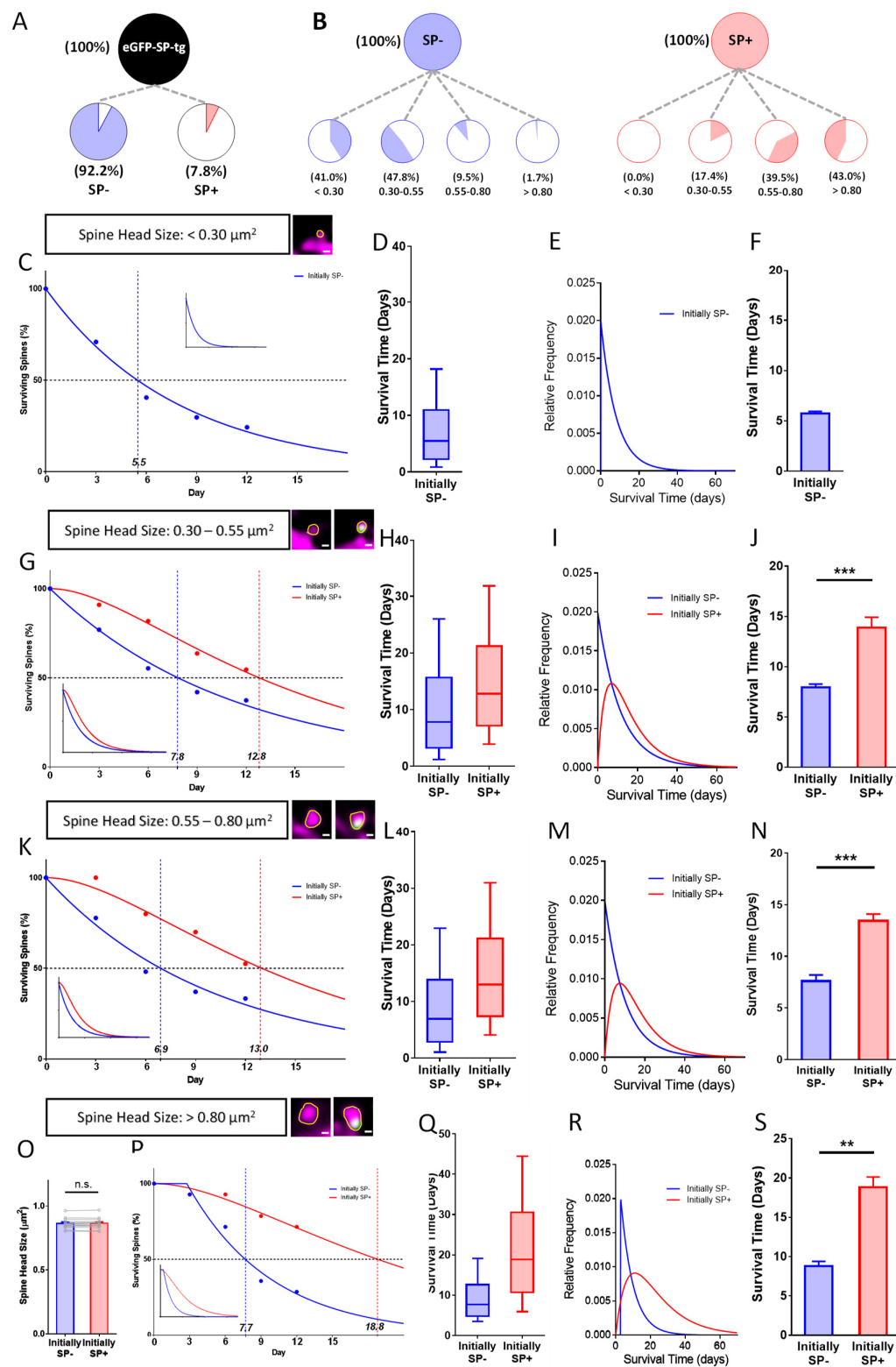
475 **Figure 5. Presence of SP in spines determines their long-term survival.** (A) Fraction of SP- (≈ 92.2%) and SP+
476 spines (≈ 7.8%) in eGFP-SP-tg granule cells on day 0. Number of SP+ spines = 87, SP- spines = 1021, obtained from
477 entire imaged segments; number of cultures: eGFP-SP-tg = 24. (B) SP- (blue) and SP+ spines (red) were divided
478 into four size classes: very small (< 0.3µm^2), small (0.3-0.55 µm^2), medium (0.55-0.8 µm^2) and large (> 0.8 µm^2)
479 spines. Whereas most SP- spines were found in the very small (41.0%) and small (47.8%) spine groups, the
480 majority of SP+ spines were in the medium (39.5%) and large (43.0%) size groups. (C) Survival curve of very small
481 spines (example shown) from day 0 until day 12. Dots: observed fractions; curves: fitted to observation points.
482 SP- spines (blue line) followed a single exponential decay curve (median survival ≈ 5.5 days). Inset: extrapolated
483 decay curve until day 70. Number of very small SP- spines = 148. (D) Survival time of the total population of SP-
484 spines derived from the fitted survival curve. Box indicates median, lower and upper quartiles. Whiskers indicate
485 10th and 90th percentiles, respectively. (E) Relative frequency distribution of very small SP- spines. (F) Mean
486 survival time of very small SP- spines; computational model; 10 samples, 148 SP- spines. (G) Survival curves of
487 small SP- and SP+ spines (examples shown). SP- spines (blue line; median survival ≈ 7.8 days) followed a single
488 exponential decay curve, SP+ spines (red line; median survival ≈ 12.8 days) followed a conditional two-stage
489 decay curve. Inset: extrapolated decay curves until day 70. Number of SP- spines = 217; SP+ spines = 11. (H)
490 Survival times and (I) relative frequency distributions of small SP- and SP+ spines. (J) Mean survival time of SP+
491 spines compared to SP- spines; computational model. ***p = 0.0003, Mann-Whitney U-test. 10 samples; 11 SP+
492 and 217 SP- spines. (K) Survival curves of medium sized SP- and SP+ spines (examples shown). SP- spines (blue
493 line; median survival ≈ 6.9 days) followed a single exponential decay curve, SP+ spines (red line; median survival
494 ≈ 12.9 days) followed a conditional two-stage decay curve. Inset: extrapolated decay curves until day 70. Number
495 of SP- spines = 27; SP+ spines = 40. (L) Survival times and (M) relative frequency distributions of medium SP- and
496 SP+ spines. (N) Mean survival time of SP+ spines compared to SP- spines; computational model. ***p < 0.0001,
497 Mann-Whitney U-test. 10 samples; 40 SP+ and 27 SP- spines. (O) SP+ and SP- spines were size-matched in the
498 largest spine group (mean spine head sizes; not significant; p = 0.475, Wilcoxon matched-pairs signed rank test).
499 Number of size-matched pairs n = 14. (P) Survival curves of size-matched large SP- and SP+ spines (examples
500 shown). SP- spines (blue line; median survival ≈ 7.7 days) followed a single exponential decay curve, SP+ spines
501 (red line; median survival ≈ 18.8 days) followed a conditional two-stage decay curve. Inset: calculated decay
502 curves until day 70. (Q) Survival times and (R) relative frequency distributions of large SP- and SP+ spines. (S)
503 Mean survival time of SP+ spines compared to SP- spines; computational model. ***p < 0.0001, Mann-Whitney
504 U-test. 10 samples; 14 SP+ and 14 SP- spines.

505

506 In the small spine group ~47.8% of all SP- and ~17.4% of all SP+ spines are found (Fig. 5B), with SP+

507 spines representing ~5% of all spines in this group. Compared to the SP- spines, which followed a single

508 exponential decay curve, SP+ spines showed a longer survival time and followed a conditional double

509 phase exponential decay function (Fig. 5G-J). In the group of medium-sized spines ~9.5% of SP- and

510 ~39.5% of SP+ spines are found, with SP+ spines representing ~60% of the spines in this size group.

511 Again, SP- spines followed a single exponential decay curve, whereas SP+ spines showed longer survival

512 times and their decay was compatible with a conditional double phase exponential decay function (Fig.

513   5K-N). We conclude from these data that small and medium-sized spines survive longer and follow a

514   conditional double-phase decay kinetic if SP is present.

515   Finally, we looked at the population of large spines. Although these spines only account for ~4.9% of

516   all spines, they are considered especially important in the context of memory storage (Segal, 2005;

517   Bourne and Harris, 2007; Kasai et al., 2010; McKinney, 2010; Abdou et al., 2018). In this group of spines

518   only ~1.7% of the SP- spines are found whereas ~43% of SP+ spines are part of this subgroup. SP+

519   spines represent ~65% of the spines in this size group. Comparing spine pairs of equal head sizes (Fig.

520   5O) major differences in their survival and decay kinetics were revealed: Whereas SP-spines followed

521   a single exponential function, SP+ spines were best modelled using the conditional double-phase decay

522   function (Fig. 5P-S). We conclude that large SP- spines are pruned fast. Their survival is comparable to

523   that of very small (Fig. 5C), small (Fig. 5G) and medium sized (Fig. 5K) spines, suggesting that it is the

524   presence of SP within spines rather than spine size per se which determines long-term spine survival.

525   <u>Synaptopodin-deficiency alters spine survival</u>

526   We then turned to SP-deficient mice to study spine survival in the absence of SP. (Fig. 6). First, we

527   compared the distribution of spines of the eGFP-SP-tg and the SP-KO mice and found comparable

528   fractions of spines in the four size categories (Fig. 6A). This is in line with our observation that SP-

529   deficiency does not affect average spine head size or spine head distribution in vivo (c.f. Fig. 1C, D) or

530   in vitro (c.f. Fig. 2E, F). Next, we compared SP-deficient spines to SP- spines and found that these two

531   groups of spines behave very similar with regard to their survival times and decay kinetics in each of

532   the four size groups (Fig. 6B-R): survival times were similar and all curves followed single exponential

533   decay functions. This demonstrates that the "spine phenotype" associated with SP-deficiency does not

534   result in altered spine geometry but in altered spine survival, i.e. spine stability.

535   We then wondered how the lack of the stable SP+ spine population affects spine dynamics, in particular
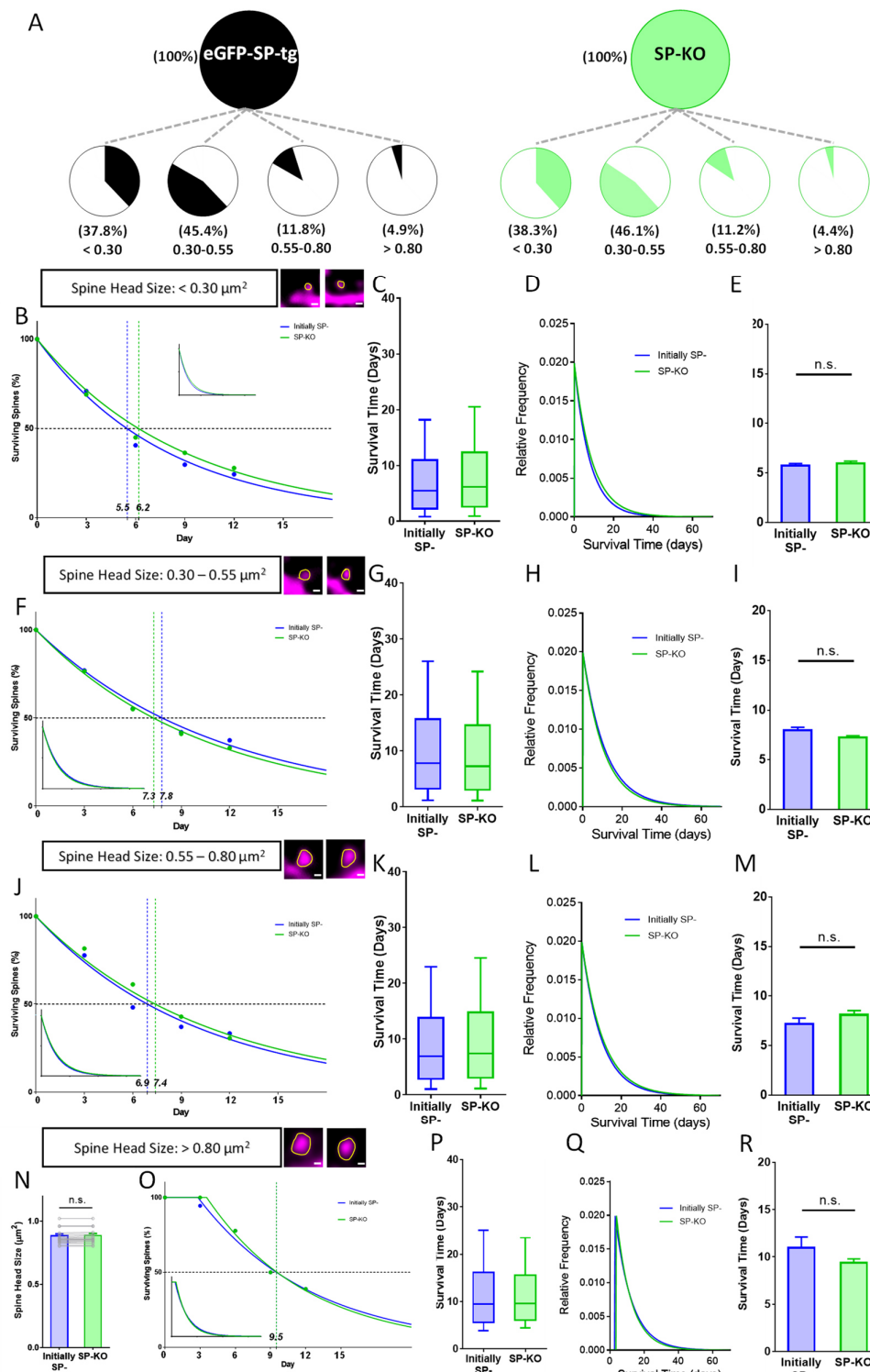
536   spine turnover, of the SP-deficient animals.

Figure 6. Spines of SP-deficient mice decay like SP- spines. (A) Spine head size distributions of granule cell dendrites of eGFP-SP-tg and SP-KO mice were similar. Number of spines: eGFP-SP-tg = 1107; SP-KO = 1113, obtained from entire imaged segments; number of cultures: eGFP-SP-tg = 24; SP-KO = 21. (B) Survival curve of

541 very small spines (examples shown) from day 0 until day 12. Dots: observed fractions; curves: fitted to
542 observation points. SP- spines (blue line; median survival ≈ 5.5 days) and spines of SP-KO-mice (green line; median
543 survival ≈ 6.2 days) followed single exponential decay curves. Inset: calculated decay curves until day 70. Number
544 of SP- spines = 148; SP-KO spines = 187. (C) Calculated survival times and (D) relative frequency distributions of
545 very small SP- and SP-KO spines. (E) Mean survival time of very small SP- and SP-KO spines; computational model.
546 p = 0.529, Mann-Whitney U-test. 10 samples; 148 SP-, 187 SP-KO spines. (F) Survival curves, (G) calculated
547 survival times, and (H) relative frequency distributions of small SP- and SP-KO spines. SP- spines (blue; median
548 survival ≈ 7.8 days) and SP-KO spines (green, median survival ≈ 7.4 days) followed single exponential decay
549 curves. Number of SP- spines = 217; SP-KO spines = 200. (I) Mean survival times; computational model. p = 0.089,
550 Mann-Whitney U-test. 10 samples; 217 SP-, 200 SP-KO spines. (J) Survival curves, (K) calculated survival times,
551 and (L) relative frequency distributions of medium-sized SP- and SP-KO spines. SP- spines (blue; median survival
552 ≈ 6.9 days) and SP-KO spines (green, median survival ≈ 7.4 days) followed single exponential decay curves.
553 Number of SP- spines = 27; SP-KO spines = 49. (M) Mean survival times; computational model. p = 0.280, Mann-
554 Whitney U-test. 10 samples; 27 SP-, 49 SP-KO spines. (N) SP+ and SP- spines were size-matched in the largest
555 spine group (mean spine head sizes; not significant, p = 0.109, Wilcoxon matched-pairs signed rank test. Number
556 of size-matched pairs n = 18. (O) Survival curves, (P) calculated survival times, and (Q) relative frequency
557 distributions of large SP- and SP-KO spines. SP- spines (blue; median survival ≈ 9.5 days) and SP-KO spines (green,
558 median survival ≈ 9.5 days) followed single exponential decay curves. Number of size-matched pairs = 18. (R)
559 Mean survival times; computational model. p = 0.393, Mann-Whitney U-test. 10 samples; 18 SP- and 18 SP-KO
560 spines.

561 The following figure supplements are available for Figure 6.
562 **Figure S2 related to Figure 6. SP-KO mice compensate for the loss of SP with an increased spine formation and**
563 **an increased turnover ratio.**

564

565 We reasoned that the reduced stability of large spines will have to be homeostatically compensated

566 by an increased formation of spines and an increased spine turnover. Indeed, these dynamic

567 parameters were significantly increased (Suppl. Fig. 2 related to Fig. 6), revealing a yet unknown

568 phenotype of the SP-deficient mutants.

569 <u>Spines shrink and pass through a SP-negative stage before pruning</u>

570 After investigating the survival of individual spines considering only their initial SP content (SP+ or SP-

571 ; previous paragraphs), we determined changes of the SP+ and SP- spine populations with regard to

572 survival, head size and SP content (Fig. 7). For this, all spines were identified on day 0 as being either

573 SP+ or SP-. For each of the following observation time points, these spines were categorized as either
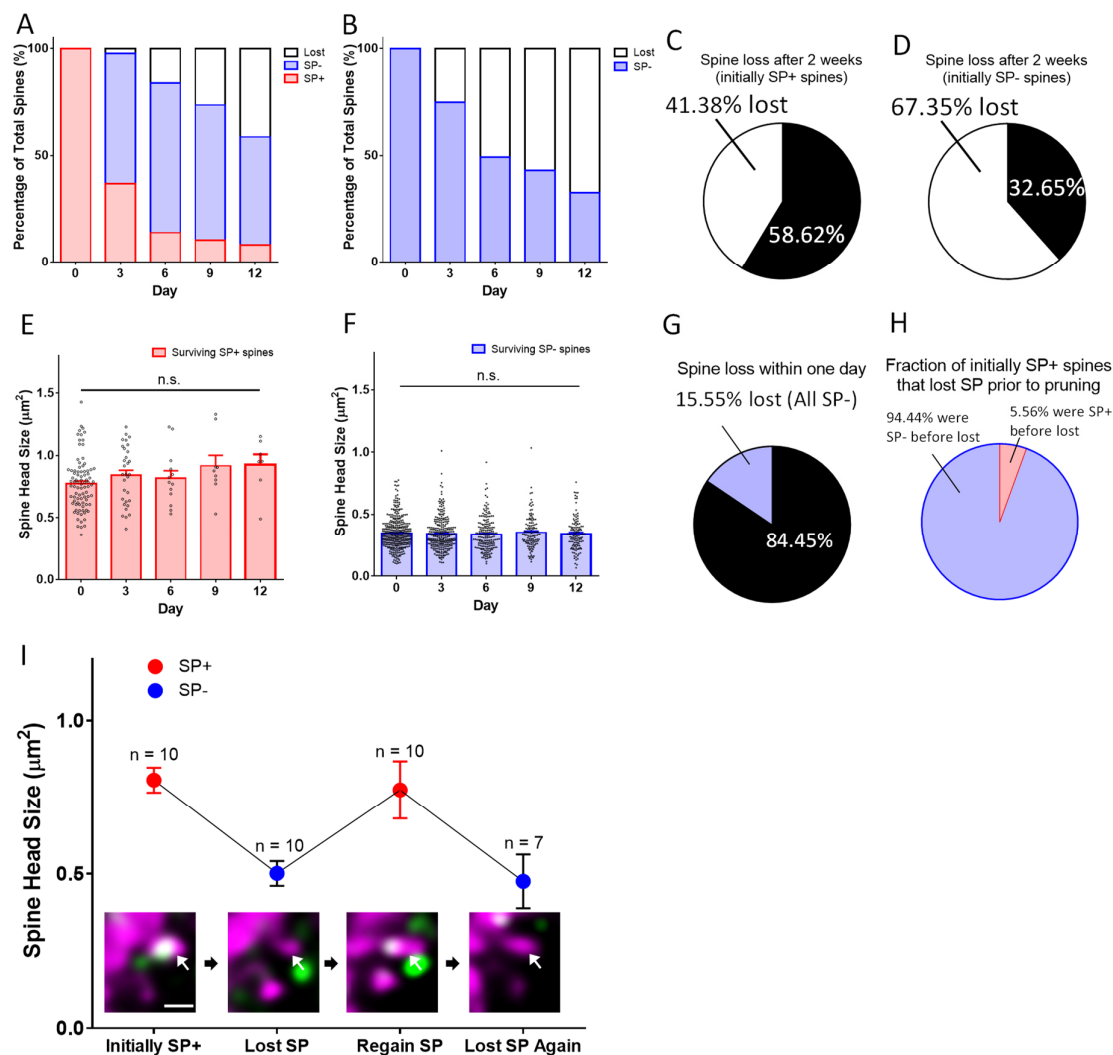
574 SP+, SP- or "lost" (Fig. 7A, B).

575

Figure 7. Spines pass through a SP-negative state before pruning. (A, B) The fates of (A) a group of SP+ spines (n = 87) and (B) a group of SP- spines (n = 392) are illustrated. SP+ spines gradually become SP- or disappear. SP-spines disappear with time. (C, D) Fractions of (C) SP+ and (D) SP- spines surviving for two weeks. (E, F) Mean spine head sizes of surviving (E) SP+ and (F) SP- spines. Spine head sizes were not significantly different (SP+ spines, p = 0.115; SP- spines, p = 0.627, Kruskal-Wallis test). (G) Analysis of SP content of all spines lost within one day (days -1 to 0; n = 72; 15.55% of 463 spines). All pruned spines were SP-. (H) Analysis of all SP+ spines that were pruned during the observation period. Most spines (n = 34) went through a SP- state before disappearing, a minority (n = 2) was lost directly between imaging days 0 and 3. (I) A subpopulation of SP+ spines undulated between SP+ and SP- states (n = 10). The gain or loss of SP was accompanied by an increase or decrease of spine head size, respectively. An example for such a case is illustrated (arrow in insets). Scale bar = 1 μm.

The following figure supplements are available for Figure 7.

Figure S3 related to Figure 7. Time-lapse 2-photon imaging data of individual SP+ spines.

Figure S4 related to Figure 7. Time-lapse 2-photon imaging data of individual SP- spines.

Figure S5 related to Figure 7. Time-lapse 2-photon imaging data of individual spines undulating between SP+ and SP- states.

591   In addition, the spine head sizes of the surviving SP+ (Fig. 7E) and SP- (Fig. 7F) spines were analyzed for

592   each time point. Spines that repeatedly changed their SP content were excluded and analyzed

593   separately (see below).

594   This analysis revealed that in the group of initially SP+ spines the fraction of SP+ spines decreased with

595   time whereas the fraction of SP- spines increased. This was followed by an increase in the fraction of

596   lost spines (Fig. 7A). In the group of the initially SP- spines the fraction of surviving spines decreased

597   much more rapidly (Fig. 7B). At the observation endpoint (day 12), ~59% of spines which were initially

598   SP+ survived (Fig. 7C), whereas only ~33% of spines which were initially SP- were still present (Fig 7D).

599   The size of the surviving SP+ (Fig. 7E) and SP- (Fig. 7F) spines did not change significantly during the

600   two-week observation period, in line with our finding that spine head size per se is not a major

601   determinant of spine stability.

602   We then looked specifically at the spines that were lost, since our analysis had revealed a shift from

603   SP+ spines to SP- spines (Fig. 7A). This shift suggested that SP+ spines go through a SP- state before

604   pruning. Since we followed the fate and the SP content of every spine over the two-week imaging time

605   period (Suppl. Figs. 3, 4 related to Fig. 7), we could test this hypothesis. First, we determined the SP

606   content of the 16% of spines that were lost within one day, i.e. between days -1 and 0. All of these

607   pruned spines were SP-, in line with our hypothesis (Fig. 7G). Next, we predicted that SP+ spines should

608   not be lost without going through a SP- state. For this analysis, we looked at all spines that were initially

609   SP+, i.e. spines SP+ at day 0, and focused on those SP+ spines that were pruned sometime during the

610   observation period. Of these spines ~94% were SP- prior to their pruning (Fig. 7H). In the rare cases

611   (n=2; ~6%), in which a SP+ spine seemingly disappeared without passing through a SP- state, the two

612   observation time points were several days apart (e.g., between day 0-3; Suppl. Fig. 3 related to Fig. 7),

613   making it highly likely that we missed a transitory SP- state of these spines prior to their pruning.

614

615   <u>Loss of SP from spines is not sufficient to cause pruning</u>

616   After finding the above evidence that SP is removed from spines prior to their pruning, we wondered

617   whether removal of SP from a spine is inexorably followed by the loss of this spine. If this were the

618   case all SP+ spines losing their SP cluster should disappear. This hypothesis could be falsified, since we

619   observed several SP+ spines (n=10) undulating between a SP+ and SP- state (Fig. 7I). Thus, SP can be

620   removed from a spine and reintroduced into a spine without the spine being pruned. Of note, the

621   changes in SP content were accompanied by bidirectional changes in head size (Fig. 7I, Suppl. Fig. 5

622   related to Fig. 7). We also observed SP- spines, which became SP+, lost SP, and became SP+ again at a

623   later stage (n=8; data not shown). Taken together, we conclude from these observations that loss of a

624   SP cluster from a spine is not sufficient to cause pruning of that spine.

625   <u>Mathematical simulations of spine stability are compatible with a conditional two-stage decay process</u>

626   The decay curves of SP- and SP+ spines (Fig. 4, 5) are non-overlapping and mathematically distinct since

627   they cannot be trivially transformed into each other, e.g. using a scaling factor. We first analyzed the

628   survival curve of SP- spines, which we could readily simulate and fit to our data using a one-phase

629   exponential decay function:

630
$$Y = 100\% * \exp\left(-\frac{t - offset}{\tau spine}\right)$$

631   In this equation, the variable Y denotes the percentage of SP- spines surviving up to day t starting with

632   100% SP- spines present at day zero. τspine denotes the decay time constant of spine loss. The half-

633   life of spines was determined as 0.69*τspine. "offset" denotes the start of the decay. Fitting the data

634   to this model, τspine of SP- spines is ~9.8 days and the half-life of these spines is ~6.8 days (Fig. 4). Size

635   matched SP- spines (Fig. 4G, H), SP- spines of different sizes (Fig. 5), and SP-deficient spines (Fig. 6)

636   followed similar one-phase exponential decay functions.

33

637   In contrast, the survival curve of SP+ spines did not follow a one-phase exponential decay function. An

638   almost perfect fit could be obtained, however, by using a conditional double phase exponential decay

639   function, identical to the one used to model the conditional two-stage decay of radioisotopes

640   (Bateman, 1910). In this model, a radioisotope undergoes decay and forms an instable intermediary.

641   This intermediary decays again into a stable isotope. The two decay processes have different decay

642   time constants. We now applied this function to the data obtained for spine survival: SP+ spines were

643   considered to lose SP with the time constant τSP. The new SP- spine would then disappear with the

644   time constant τspine, i.e. the same time constant determined for the SP- spines above:

645
$$Y = 100\% * \left(\frac{\exp\left(\frac{-t}{\tau spine}\right)}{\tau SP * \left(\frac{1}{\tau SP} - \frac{1}{\tau spine}\right)} + \frac{\exp\left(\frac{-t}{\tau SP}\right)}{\tau SP * \left(\frac{1}{\tau spine} - \frac{1}{\tau SP}\right)} + \exp\left(\frac{-t}{\tau SP}\right) \right)$$

646   In this equation, the variable Y denotes the percentage of SP- spines surviving up to day t starting with

647   100% of SP+ spines present at day zero. We fitted the survival data for SP+ spines to this equation and

648   found the time constant τSP of the first decay process (SP+ spines becoming SP-) to be ~11.1 days and

649   accordingly the half-life of SP in spines to be ~7.7 days. Thus, after approximately 17.4 days, ~50% of

650   all initially SP+ spines would have disappeared (Fig. 4). Size matched SP+ spines (Fig. 4G, H) and SP+

651   spines of different sizes (Fig. 5) followed similar conditional double phase exponential decay functions.

652   We conclude from this mathematical analysis of our experimental data that the survival curves of SP+

653   spines are compatible with a conditional two-stage decay process in which SP+ spines first lose their

654   SP cluster (τSP) before being subsequently pruned as SP- spines with the time constant (τspine; same

655   as initially SP- spines; Fig. 8).
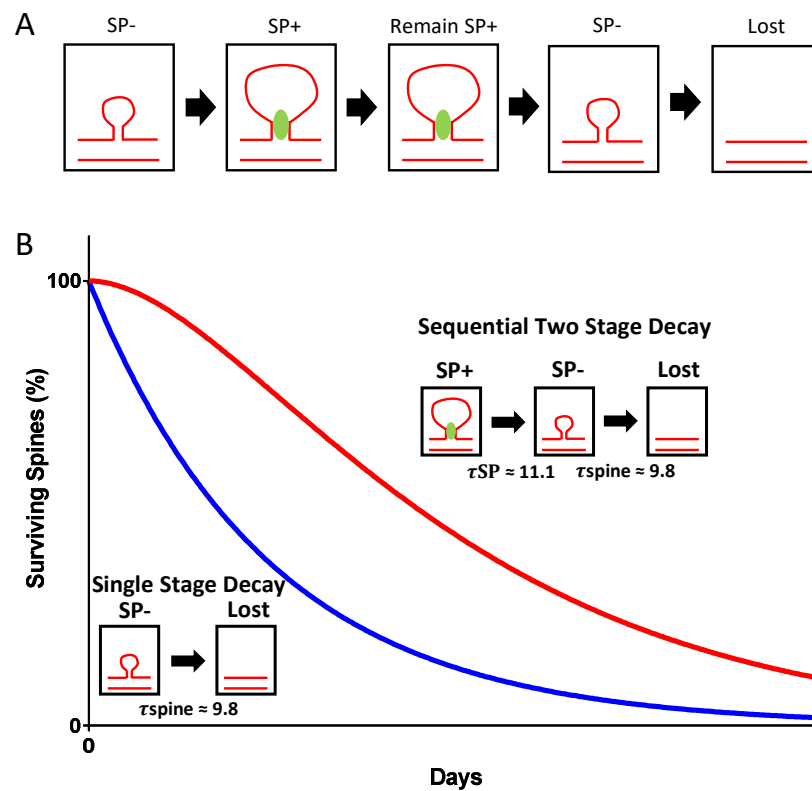
Figure 8. Model illustrating the role of SP in spine head size and spine stability. (A) SP- spines gaining SP show a concomitant increase in spine head size. SP in spines stabilizes spines. Prior to spine loss, SP is removed from spines. Loss of SP from spines is associated with a reduction in spine head size. (B) The data of the present study suggest a conditional two-stage exponential decay model for SP+ spines. The first stage involves SP+ spines losing SP (τSP) and the second stage involves the gradual disappearance of these SP- spines (τspine). For SP- spines, our data suggest they undergo a classical single stage exponential decay model where spines are lost exponentially with time.

664 **Discussion**

665 Spine geometry and spine stability are structural parameters that have been linked to synaptic

666 strength, network reorganization and memory trace formation (Bourne and Harris, 2007; Kasai et al.,

667 2010; McKinney, 2010; Koleske, 2013; Rogerson et al., 2014; Segal, 2017). A molecule potentially

668 involved in these biological phenomena is the actin-modulating protein SP (Mundel et al., 1997; Deller

669 et al., 2000a; Jedlicka and Deller, 2017). Using a combination of mouse genetics, viral transduction and

670 2-photon time-lapse imaging, the effects of SP on spine geometry and stability were analyzed for two

671 weeks in an organotypic environment. Our observations can be summarized as follows: (1) SP is

672 primarily present in large spines. (2) SP+ spines are more stable than SP- spines. (3) The effect of SP on

673 spine stability is independent of spine size and is seen in small as well as in large spines. (4) In SP-

674 deficient animals, spines decay like SP- spines. In these mutants, a compensatory increase in spine

675 turnover is observed. (5) Analysis of SP+ spines that were subsequently pruned revealed that these

676 spines went through a SP- state prior to their removal, following a conditional two-stage decay curve.

677 (6) Removal of SP from spines is not sufficient to induce spine pruning.

678 In sum, our results implicate SP as a major regulator of spine stability. Since SP is primarily present in

679 large spines, its presence explains why these spines have a considerably longer lifetime than small

680 spines, as reported by others (e.g., (Matsuzaki et al., 2004; Kasai et al., 2010; McKinney, 2010).

681 <u>Spine head expansion and shrinkage is correlated with SP content and SP cluster size</u>

682 SP is an actin-modulating protein (Mundel et al., 1997; Asanuma et al., 2006; Okubo-Suzuki et al.,

683 2008). Since geometry and dynamics of spines depend on F-actin-assembly and disassembly (Fischer

684 et al., 1998; Matus, 2000), a role for SP in spine motility appeared to be likely (Deller et al., 2000a).

685 Indeed, after investigations in SP-deficient mice showed that SP does not influence spine density or

686 spine length (Deller et al., 2003), a robust correlation between SP and spine head size was reported in

687 dissociated hippocampal neurons transfected with SP (Okubo-Suzuki et al., 2008; Vlachos et al., 2009)

36

688 and in acute hippocampal brain slices (Zhang et al., 2013). In our organotypic tissue culture

689 preparations we have confirmed and extended these findings and observed a strong correlation

690 between SP content and spine head size as well as between SP cluster size and spine head size.

691 Furthermore, the mean cross-sectional area of SP+ spines was found to be almost twice as large as the

692 mean cross-sectional area of SP- spines. By following single SP+ spines over several days, we could also

693 detect a group of SP-containing spines that lost and subsequently regained SP. The size of the spine

694 head shrank in spines losing SP and increased in spines regaining SP. Thus, SP content and cluster size

695 correlated with changes in spine head size in both directions. However, SP itself does not seem to

696 cause spine head-size expansion, since short-term imaging revealed that spines growing bigger heads

697 first expand their heads and subsequently insert SP (Okubo-Suzuki et al., 2008; Konietzny et al., 2019),

698 maintaining the expanded spine head (Okubo-Suzuki et al., 2008).

699 <u>The presence of SP rather than head size determines spine stability</u>

700 Spines differ with regard to their lifetime and stability. Although spines of all sizes can persist for long

701 time periods, spines with a large spine head are believed to be more stable than spines with only a

702 small head (Matsuzaki et al., 2004; Kasai et al., 2010). Alternatively, if classifications of spine shape are

703 used to categorize spines (Bourne and Harris, 2008), mushroom spines were reported to be more

704 stable than stubby or thin spines (Kasai et al., 2003; Bourne and Harris, 2007; Koleske, 2013), even

705 following denervation (Caceres and Steward, 1983). Since mushroom spines often have large spine

706 heads, a considerable overlap exists between "spines with a large spine head" and "mushroom spines",

707 explaining the similarity of the results. Regardless of these different classifications, however, spine size

708 has been considered a major determinant of spine stability (Kasai et al., 2010; McKinney, 2010).

709 Here we have investigated the molecular basis for this increased spine stability and have tested the

710 possibility that the actin-modulating protein SP (Mundel, 1998; Deller et al., 2003) could play a role.

711 Since spine stability depends on the stability of the spine actin cytoskeleton (Fischer et al., 1998; Matus,

37

712   2000), actin-modulating proteins such as SP are candidate regulators for spine motility and stability

713   (Deller et al., 2000a; Bourne and Harris, 2008). Our data revealed that SP is indeed a major regulator

714   of spine stability. Furthermore, our data also suggest that it is primarily the content of SP within a spine

715   that imparts stability to a given spine rather than the size of the spine per se. This second conclusion

716   is supported by the following: (1) Small spines (0.3-0.55 μm^2 head area) containing SP have a long

717   lifetime and a median survival of 12.8 days. Large spines (>0.8 μm^2 head area) without SP have a

718   median survival time of 7.7 days. Thus, small SP+ spines are more stable than large SP- spines. (2)

719   Comparison of the median survival times of SP- spines of all sizes (i.e., very small, small, medium and

720   large) revealed that their median survival time was similar and much shorter than the median survival

721   time of any of the SP+ spine groups. Finally, (3) all spines, including the large spines, of SP-deficient

722   animals decayed like SP- spines and had short median survival times. Although we cannot fully exclude

723   a small effect of spine size on spine survival, e.g. large spines may need time to shrink prior to their

724   removal (see next paragraph), our data clearly show that the presence of SP within a spine is a more

725   reliable indicator of its stability than its morphology alone, i.e. the size of its spine head.

726   <u>SP+ spines that are pruned pass through a SP- state and shrink in size</u>

727   Two weeks of time-lapse imaging of identified SP+ spines made it possible to study their fate: Single

728   SP+ spines surviving for the entire time period, SP+ spines losing and regaining SP, as well as SP+ spines

729   that were pruned could be identified and analyzed (Suppl. Figs. 3, 4, 5 related to Fig. 7). From these

730   multidimensional dynamic time-lapse data, we could draw additional conclusions: First, from the fact

731   that some spines lose and regain SP with time, we concluded that loss of SP from a spine is not by itself

732   sufficient to tag a spine for pruning. Rather, such spines seem to re-enter the large pool of SP- spines

733   from which new SP+ spines can be recruited. Second, by following SP+ spines that were pruned during

734   the observation period, we could show that in almost all cases, these spines went through a SP- state

735   before they disappeared. In the two cases in which SP+ spines were pruned without an intermediate

736   state, the two observation time points were several days apart (e.g. three days between day 0 and day

737   3), making it highly likely that the intermediate SP- state was missed. Thus, we conclude that removal

738   of the spine stabilizing protein SP is a necessary step before the actin-cytoskeleton of a spine can be

739   degraded and the spine can be pruned. Third, in line with the fact that SP is associated with large

740   spines, we observed that spines losing SP also shrank in size (Suppl Figs. 3-5, related to Fig 7). In the

741   case of spines changing their SP content (Suppl. Fig. 5, related to Fig. 7) this also resulted in several

742   corresponding head size changes. In agreement with these observations, we found that SP+ spines

743   designated to be pruned follow a conditional two-stage decay function, similar to the one described

744   for radioactive isotopes in Physics (Bateman, 1910): The first stage is the "decay" of SP+ spines into a

745   SP- state. The second stage of the decay is the pruning of these SP- spines, which is as fast as for other

746   spines that were primarily devoid of SP (Fig. 8).

747   <u>SP-deficient neurons homeostatically compensate for the loss of SP with increased spine formation</u>

748   The role of SP in the regulation of spine stability is further supported by data from SP-deficient mice.

749   Granule cells of these mice exhibited spines that decayed like SP- spines. In addition, SP-deficient

750   granule cells compensated for the reduced stability of spines by increasing their spine formation and

751   thereby their spine turnover ratio. This finding suggests that SP-deficient neurons homeostatically

752   compensate for the loss of stability by upregulating their spine formation. This may explain why loss

753   or overexpression of SP does not seem to affect spine densities (Deller et al., 2003; Okubo-Suzuki et

754   al., 2008; Vlachos et al., 2009). Whereas spine density appears to be regulated by other molecules,

755   including among others hormones (Woolley, 2000; Segal and Murphy, 2001; Fester et al., 2012; Luine

756   and Frankfurt, 2012), actin-modulating proteins (Yamazaki et al., 2014), Fragile X mental retardation

757   protein (Irwin et al., 2000; Bagni and Zukin, 2019), non-coding RNAs (Briz et al., 2017), neurotrophic

758   factors (Murphy et al., 1998) and adhesion molecules (Segura et al., 2007; Keeler et al., 2015; Muller

759   et al., 2017), SP appears to be a major regulator of spine stability.

760 <u>SP marks a subpopulation of stable spines - implications for synaptic plasticity and long-term memory</u>

761 The present study showed that SP is found in a subpopulation of granule cell spines that are highly

762 stable. The stabilizing effect of SP is most likely caused by its actin-modulating function: In hippocampal

763 neurons, it has been shown to protect F-actin from disruption (Okubo-Suzuki et al., 2008; Wang et al.,

764 2016) and in kidney it has been demonstrated to regulate actin organization by protecting RhoA from

765 Smurf1-mediated ubiquitination and proteasomal degradation by competing with Smurf1 for RhoA

766 binding (Asanuma et al., 2006). Since the Rho family of small GTPases regulate the maintenance of

767 spines and spine formation (Tashiro and Yuste, 2008), a similar role for SP in the CNS has been

768 suggested (Asanuma et al., 2006; Zhang et al., 2013). However, the kidney form of SP differs from the

769 neuronal form (Asanuma et al., 2006), and thus this attractive hypothesis still awaits confirmation.

770 SP also plays an important role in Hebbian- (Yamazaki et al., 2001; Deller et al., 2003; Okubo-Suzuki et

771 al., 2008; Holbro et al., 2009; Jedlicka et al., 2009; Vlachos et al., 2009; Zhang et al., 2013; Jedlicka and

772 Deller, 2017) and homeostatic (Vlachos et al., 2013) forms of synaptic plasticity. These effects on

773 plasticity may not only depend on the actin-modulating properties of SP but also on the spine

774 apparatus organelle, which requires SP for its formation (Deller et al., 2003). The spine apparatus is

775 part of the effector machinery needed for changing synaptic strength at excitatory postsynapses

776 (Jedlicka and Deller, 2017). It acts as a calcium source and sink within spines (Vlachos et al., 2009;

777 Korkotian and Segal, 2011; Korkotian et al., 2014) and is required for AMPA-R trafficking to the

778 postsynapse (Vlachos et al., 2009). Thus, SP appears to be involved in at least four biological

779 phenomena linked to changes in synaptic strength and in the maintenance of such a change, i.e.

780 prolonged spine head expansion (Okubo-Suzuki et al., 2008; Vlachos et al., 2009; Zhang et al., 2013),

781 spine stabilization (this study), calcium release from intracellular stores (Vlachos et al., 2009; Korkotian

782 and Segal, 2011; Korkotian et al., 2014) and AMPA-R trafficking (Vlachos et al., 2009), demonstrating

40

783   its important role as a plasticity-related protein. Conversely, the presence of SP in spines identifies

784   spines that are stable, large and strong.

785   At the network level, strong and stable synapses are considered the backbone of long-term memory

786   (Kasai et al., 2010; Koleske, 2013; Rogerson et al., 2014; Segal, 2017). Neurons connected by such

787   synapses form ensembles of cells that are in turn essential for memory engrams (Yokose et al., 2017).

788   Indeed, as has been shown recently, the sharing of engram cells can link memories, whereas synapse-

789   specific plasticity guarantees the identity and storage of individual memories (Abdou et al., 2018). In

790   the present study, we report that the stability of spines critically depends on the presence of the actin-

791   modulating protein SP within a spine. This makes it attractive to speculate that synapses requiring a

792   high degree of stability, such as those synapses binding excitatory neurons together into functional

793   ensembles, require SP as their stabilizer. Conversely, SP may be an attractive marker for such synapses,

794   as it allows for their identification in vitro and possibly also in vivo. Using optogenetic approaches, such

795   as the one employed by Abdou and co-workers (Abdou et al., 2018), the role of SP+ spines in memory

796   formation can now be addressed.

Cited References

Abdou K, Shehata M, Choko K, Nishizono H, Matsuo M, Muramatsu SI, Inokuchi K (2018) Synapse-specific representation of the identity of overlapping memory engrams. Science 360:1227-1231.

Asanuma K, Yanagida-Asanuma E, Faul C, Tomino Y, Kim K, Mundel P (2006) Synaptopodin orchestrates actin organization and cell motility via regulation of RhoA signalling. NatCell Biol 8:485-491.

Asanuma K, Kim K, Oh J, Giardino L, Chabanis S, Faul C, Reiser J, Mundel P (2005) Synaptopodin regulates the actin-bundling activity of α-actinin in an isoform-specific manner. Journal of Clinical Investigation 115:1188-1198.

Bagni C, Zukin RS (2019) A Synaptic Perspective of Fragile X Syndrome and Autism Spectrum Disorders. Neuron 101:1070-1088.

Bas Orth C, Vlachos A, Del Turco D, Burbach GJ, Haas CA, Mundel P, Feng G, Frotscher M, Deller T (2005) Lamina-specific distribution of Synaptopodin, an actin-associated molecule essential for the spine apparatus, in identified principal cell dendrites of the mouse hippocampus. JCompNeurol 487:227-239.

Bateman H (1910) Solution of a system of differential equations occurring in the theory of radioactive transformations. Proc Camb Philos Soc 15:423-427.

Bourne J, Harris KM (2007) Do thin spines learn to be mushroom spines that remember? Current opinion in neurobiology 17:381-386.

Bourne JN, Harris KM (2008) Balancing structure and function at hippocampal dendritic spines. AnnuRevNeurosci 31:47-67.

Briz V, Restivo L, Pasciuto E, Juczewski K, Mercaldo V, Lo AC, Baatsen P, Gounko NV, Borreca A, Girardi T, Luca R, Nys J, Poorthuis RB, Mansvelder HD, Fisone G, Ammassari-Teule M, Arckens L, Krieger P, Meredith R, Bagni C (2017) The non-coding RNA BC1 regulates experience-dependent structural plasticity and learning. Nature communications 8:293.

Caceres A, Steward O (1983) Dendritic reorganization in the denervated dentate gyrus of the rat following entorhinal cortical lesions: a Golgi and electron microscopic analysis. JCompNeurol 136:287-295.

Cugno A, Bartol TM, Sejnowski TJ, Iyengar R, Rangamani P (2018) Geometric principles of secondary messenger dynamics in dendritic spines. bioRxiv doi: https://www.biorxiv.org/content/10.1101/444489v1.

Del Turco D, Deller T (2007) Organotypic entorhino-hippocampal slice cultures--a tool to study the molecular and cellular regulation of axonal regeneration and collateral sprouting in vitro. Methods MolBiol 399:55-66.

Deller T, Mundel P, Frotscher M (2000a) Potential role of synaptopodin in spine motility by coupling actin to the spine apparatus. Hippocampus 10:569-581.

Deller T, Merten T, Roth SU, Mundel P, Frotscher M (2000b) Actin-associated protein synaptopodin in the rat hippocampal formation: localization in the spine neck and close association with the spine apparatus of principal neurons. JCompNeurol 418:164-181.

Deller T, Korte M, Chabanis S, Drakew A, Schwegler H, Stefani GG, Zuniga A, Schwarz K, Bonhoeffer T, Zeller R, Frotscher M, Mundel P (2003) Synaptopodin-deficient mice lack a spine apparatus and show deficits in synaptic plasticity. ProcNatlAcadSciUSA 100:10494-10499.

839   Faul C, Asanuma K, Yanagida-Asanuma E, Kim K, Mundel P (2007) Actin up: regulation of podocyte
840   structure and function by components of the actin cytoskeleton. Trends Cell Biol 17:428-437.

841   Fester L, Prange-Kiel J, Zhou L, Blittersdorf BV, Bohm J, Jarry H, Schumacher M, Rune GM (2012)
842   Estrogen-regulated synaptogenesis in the hippocampus: sexual dimorphism in vivo but not in
843   vitro. J Steroid Biochem Mol Biol 131:24-29.

844   Fischer M, Kaech S, Knutti D, Matus A (1998) Rapid actin-based plasticity in dendritic spines. Neuron
845   20:847-854.

846   Germroth P, Schwerdtfeger WK, Buhl EH (1989) Morphology of identified entorhinal neurons
847   projecting to the hippocampus. a light microscopical study combining retrograde tracing and
848   intracellular injection. Neuroscience 30:683-691.

849   Gray EG (1959) Axo-somatic and axo-dendritic synapses of the cerebral cortex: an electron microscopic
850   study. JAnat 83:420-433.

851   Grimm D, Kern A, Rittner K, Kleinschmidt JA (1998) Novel tools for production and purification of
852   recombinant adenoassociated virus vectors. Hum Gene Ther 9:2745-2760.

853   Hick M, Herrmann U, Weyer SW, Mallm JP, Tschape JA, Borgers M, Mercken M, Roth FC, Draguhn A,
854   Slomianka L, Wolfer DP, Korte M, Muller UC (2015) Acute function of secreted amyloid
855   precursor protein fragment APPsalpha in synaptic plasticity. Acta Neuropathol 129:21-37.

856   Holbro N, Grunditz A, Oertner TG (2009) Differential distribution of endoplasmic reticulum controls
857   metabotropic signaling and plasticity at hippocampal synapses. Proc Natl Acad Sci U S A
858   106:15055-15060.

859   Holtmaat A, Bonhoeffer T, Chow DK, Chuckowree J, De Paola V, Hofer SB, Hubener M, Keck T, Knott G,
860   Lee WC, Mostany R, Mrsic-Flogel TD, Nedivi E, Portera-Cailliau C, Svoboda K, Trachtenberg JT,
861   Wilbrecht L (2009) Long-term, high-resolution imaging in the mouse neocortex through a
862   chronic cranial window. Nat Protoc 4:1128-1144.

863   Irwin SA, Galvez R, Greenough WT (2000) Dendritic spine structural anomalies in fragile-X mental
864   retardation syndrome. Cereb Cortex 10:1038-1044.

865   Jedlicka P, Deller T (2017) Understanding the role of synaptopodin and the spine apparatus in Hebbian
866   synaptic plasticity - New perspectives and the need for computational modeling. Neurobiol
867   Learn Mem 138:21-30.

868   Jedlicka P, Schwarzacher SW, Winkels R, Kienzler F, Frotscher M, Bramham CR, Schultz C, Bas OC, Deller
869   T (2009) Impairment of in vivo theta-burst long-term potentiation and network excitability in
870   the dentate gyrus of synaptopodin-deficient mice lacking the spine apparatus and the cisternal
871   organelle. Hippocampus 19:130-140.

872   Kasai H, Matsuzaki M, Noguchi J, Yasumatsu N, Nakahara H (2003) Structure-stability-function
873   relationships of dendritic spines. Trends Neurosci 26:360-368.

874   Kasai H, Fukuda M, Watanabe S, Hayashi-Takagi A, Noguchi J (2010) Structural dynamics of dendritic
875   spines in memory and cognition. Trends Neurosci 33:121-129.

876   Keeler AB, Molumby MJ, Weiner JA (2015) Protocadherins branch out: Multiple roles in dendrite
877   development. Cell Adh Migr 9:214-226.

878   Koleske AJ (2013) Molecular mechanisms of dendrite stability. Nature reviews Neuroscience 14:536-
879   550.

880 Konietzny A, Bar J, Mikhaylova M (2017) Dendritic Actin Cytoskeleton: Structure, Functions, and
881   Regulations. Frontiers in cellular neuroscience 11:147.

882 Konietzny A, Gonzalez-Gallego J, Bar J, Perez-Alvarez A, Drakew A, Demmers JAA, Dekkers DHW,
883   Hammer JA, 3rd, Frotscher M, Oertner TG, Wagner W, Kneussel M, Mikhaylova M (2019)
884   Myosin V regulates synaptopodin clustering and localization in the dendrites of hippocampal
885   neurons. J Cell Sci 132.

886 Korkotian E, Segal M (2011) Synaptopodin regulates release of calcium from stores in dendritic spines
887   of cultured hippocampal neurons. J Physiol 589:5987-5995.

888 Korkotian E, Frotscher M, Segal M (2014) Synaptopodin regulates spine plasticity: mediation by calcium
889   stores. The Journal of neuroscience : the official journal of the Society for Neuroscience
890   34:11641-11651.

891 Kremerskothen J, Plaas C, Kindler S, Frotscher M, Barnekow A (2005) Synaptopodin, a molecule
892   involved in the formation of the dendritic spine apparatus, is a dual actin/alpha-actinin binding
893   protein. JNeurochem 92:597-606.

894 Luine VN, Frankfurt M (2012) Estrogens facilitate memory processing through membrane mediated
895   mechanisms and alterations in spine density. Front Neuroendocrinol 33:388-402.

896 Matsuzaki M, Honkura N, Ellis-Davies GC, Kasai H (2004) Structural basis of long-term potentiation in
897   single dendritic spines. Nature 429:761-766.

898 Matus A (2000) Actin-based plasticity in dendritic spines. Science 290:754-758.

899 McKinney RA (2010) Excitatory amino acid involvement in dendritic spine formation, maintenance and
900   remodelling. J Physiol 588:107-116.

901 Muller UC, Deller T, Korte M (2017) Not just amyloid: physiological functions of the amyloid precursor
902   protein family. Nature reviews Neuroscience 18:281-298.

903 Mundel P (1998) [Synaptopodin: an actin-associated protein of telencephalic dendrites and of
904   podocytes in the kidney glomerulus]. Annals of anatomy = Anatomischer Anzeiger : official
905   organ of the Anatomische Gesellschaft 180:391-392.

906 Mundel P, Heid HW, Mundel TM, Kruger M, Reiser J, Kriz W (1997) Synaptopodin: an actin-associated
907   protein in telencephalic dendrites and renal podocytes. JCell Biol 139:193-204.

908 Murphy DD, Cole NB, Segal M (1998) Brain-derived neurotrophic factor mediates estradiol-induced
909   dendritic spine formation in hippocampal neurons. ProcNatlAcadSciUSA 95:11412-11417.

910 Okubo-Suzuki R, Okada D, Sekiguchi M, Inokuchi K (2008) Synaptopodin maintains the neural activity-
911   dependent enlargement of dendritic spines in hippocampal neurons. MolCell Neurosci 38:266-
912   276.

913 Pologruto TA, Sabatini BL, Svoboda K (2003) ScanImage: flexible software for operating laser scanning
914   microscopes. Biomed Eng Online 2:13.

915 Radic T, Jungenitz T, Singer M, Beining M, Cuntz H, Vlachos A, Deller T, Schwarzacher SW (2017) Time-
916   lapse imaging reveals highly dynamic structural maturation of postnatally born dentate
917   granule cells in organotypic entorhino-hippocampal slice cultures. Scientific reports 7:43724.

918 Rogerson T, Cai DJ, Frank A, Sano Y, Shobe J, Lopez-Aranda MF, Silva AJ (2014) Synaptic tagging during
919   memory allocation. Nature reviews Neuroscience 15:157-169.

Schindelin J, Arganda-Carreras I, Frise E, Kaynig V, Longair M, Pietzsch T, Preibisch S, Rueden C, Saalfeld S, Schmid B, Tinevez JY, White DJ, Hartenstein V, Eliceiri K, Tomancak P, Cardona A (2012) Fiji: an open-source platform for biological-image analysis. Nature methods 9:676-682.

Segal M (2005) Dendritic spines and long-term plasticity. NatRevNeurosci 6:277-284.

Segal M (2017) Dendritic spines: Morphological building blocks of memory. Neurobiol Learn Mem 138:3-9.

Segal M, Murphy D (2001) Estradiol induces formation of dendritic spines in hippocampal neurons: functional correlates. Horm Behav 40:156-159.

Segura I, Essmann CL, Weinges S, Acker-Palmer A (2007) Grb4 and GIT1 transduce ephrinB reverse signals modulating spine morphogenesis and synapse formation. Nat Neurosci 10:301-310.

Spacek J (1985) Three-dimensional analysis of dendritic spines. II. Spine apparatus and other cytoplasmic components. Anatomy and Embryology 171:235-243.

Tashiro A, Yuste R (2008) Role of Rho GTPases in the morphogenesis and motility of dendritic spines. Methods Enzymol 439:285-302.

Vlachos A, Bas Orth C, Schneider G, Deller T (2012) Time-lapse imaging of granule cells in mouse entorhino-hippocampal slice cultures reveals changes in spine stability after entorhinal denervation. The Journal of comparative neurology 520:1891-1902.

Vlachos A, Korkotian E, Schonfeld E, Copanaki E, Deller T, Segal M (2009) Synaptopodin regulates plasticity of dendritic spines in hippocampal neurons. JNeurosci 29:1017-1033.

Vlachos A, Ikenberg B, Lenz M, Becker D, Reifenberg K, Bas-Orth C, Deller T (2013) Synaptopodin regulates denervation-induced homeostatic synaptic plasticity. Proc Natl Acad Sci U S A 110:8242-8247.

Wang L, Dumoulin A, Renner M, Triller A, Specht CG (2016) The Role of Synaptopodin in Membrane Protein Diffusion in the Dendritic Spine Neck. PloS one 11:e0148310.

Woolley CS (2000) Effects of oestradiol on hippocampal circuitry. Novartis Found Symp 230:173-180; discussion 181-177.

Yamazaki H, Kojima N, Kato K, Hirose E, Iwasaki T, Mizui T, Takahashi H, Hanamura K, Roppongi RT, Koibuchi N, Sekino Y, Mori N, Shirao T (2014) Spikar, a novel drebrin-binding protein, regulates the formation and stabilization of dendritic spines. J Neurochem 128:507-522.

Yamazaki M, Matsuo R, Fukazawa Y, Ozawa F, Inokuchi K (2001) Regulated expression of an actin-associated protein, synaptopodin, during long-term potentiation. JNeurochem 79:192-199.

Yokose J, Okubo-Suzuki R, Nomoto M, Ohkawa N, Nishizono H, Suzuki A, Matsuo M, Tsujimura S, Takahashi Y, Nagase M, Watabe AM, Sasahara M, Kato F, Inokuchi K (2017) Overlapping memory trace indispensable for linking, but not recalling, individual memories. Science 355:398-403.

Yuste R (2013) Electrical compartmentalization in dendritic spines. Annu Rev Neurosci 36:429-449.

Yuste R, Denk W (1995) Dendritic spines as basic functional units of neuronal integration. Nature 375:682-684.

Yuste R, Majewska A, Holthoff K (2000) From form to function: calcium compartmentalization in dendritic spines. NatNeurosci 3:653-659.

960   Zhang XL, Poschel B, Faul C, Upreti C, Stanton PK, Mundel P (2013) Essential role for synaptopodin in
961   dendritic spine plasticity of the developing hippocampus. The Journal of neuroscience : the
962   official journal of the Society for Neuroscience 33:12510-12518.

963   **Supplementary Figures and Captions**
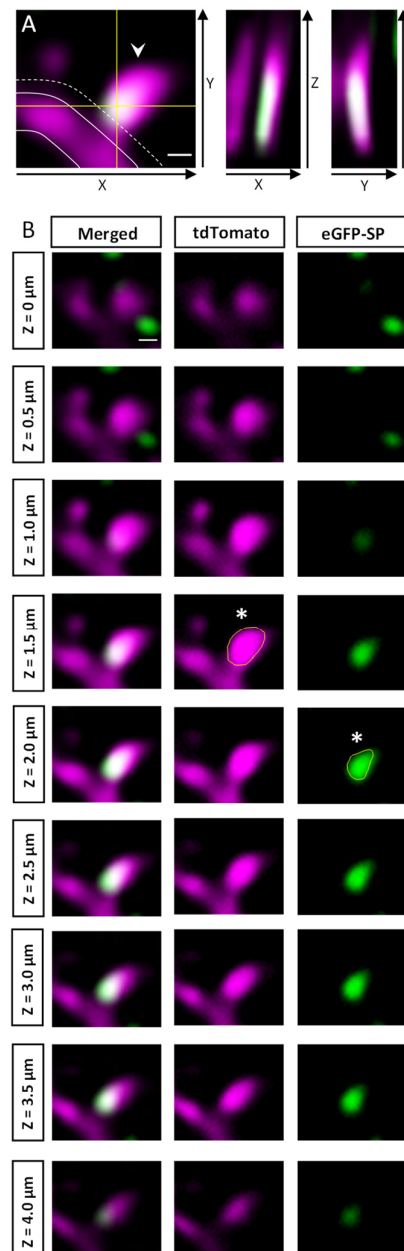
964

965   **Figure S1 related to Figure 2. Measurement of dendritic spine head size and SP cluster size.** (A) Only protrusions
966   exceeding the dendritic shaft (outlined) laterally in the x-y directions for at least 0.35 µm (dotted line) were
967   included in the analysis. Spines were considered SP+ (arrowhead) if the SP cluster overlapped with the spine
968   head and/or neck in both the x-z and y-z directions when scrolling through the z-stack. Scale bar = 0.5 µm. (B) A
969   series of x-y planes taken at consecutive z-levels is illustrated. Spine head size and SP cluster size are measured
970   by choosing the planes with the maximal cross-sectional area of the spine head and SP cluster when going
971   through the z-stack. x-y planes with the largest cross-sectional area of spine head (middle column, yellow outline
972   of spine head, asterisk) and SP cluster (right column, yellow outline of SP-cluster, asterisk) are highlighted. Scale
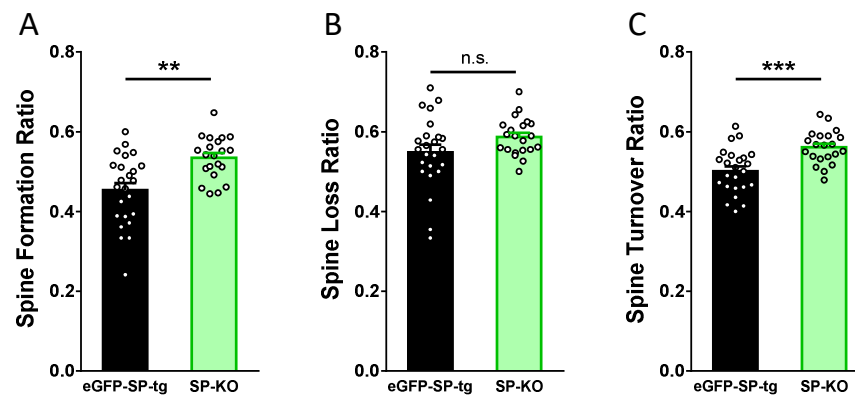973   bar = 0.5 µm.

47

974

Figure S2 related to Figure 6. SP-KO mice compensate for the loss of SP with an increased spine formation and an increased turnover ratio. (A) Spine formation was significantly higher in SP-KO dendrites as compared to eGFP-SP-tg dendrites. **$p = 0.0011$, Mann-Whitney U-test. Number of dendritic segments: eGFP-SP-tg, n = 24; SP-KO, n = 21. (B) Spine loss was not significantly different between SP-KO and eGFP-SP-tg dendrites. $p = 0.0868$, Mann-Whitney U-test. Number of dendritic segments: eGFP-SP-tg, n = 24; SP-KO, n = 21. (C) Spine turnover ratio was significantly higher in SP-KO dendrites as compared to eGFP-SP-tg dendrites over the two-week observation period. ***$p = 0.0003$, Mann-Whitney U-test. Number of dendritic segments: eGFP-SP-tg, n = 24; SP-KO, n = 21.
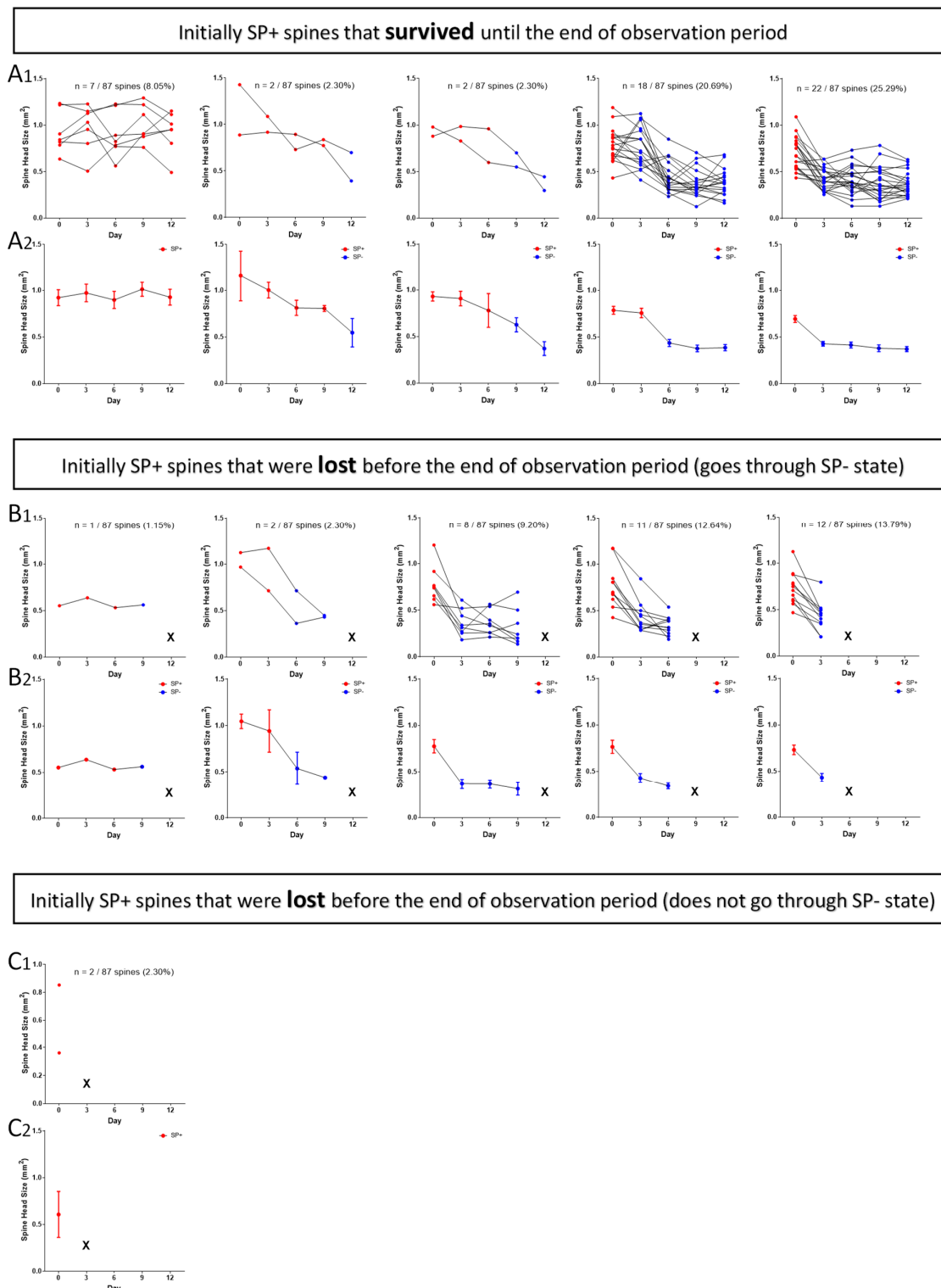
Figure S3 related to Figure 7. Time-lapse 2-photon imaging data of individual SP+ spines. SP+ spines (SP+ on day 0) were subdivided into three categories: (A) spines that survive until the end of the observation period, (B) spines that are pruned and go through a SP- state, (C) spines that are pruned without going through a SP- state

986   before pruning. The fractions, percentages and SP-content (SP+, red; SP-, blue) of spines in the different
987   categories are indicated. Upper panels (A1 through C1) show individual spines, lower panels (A2 through C2)
988   show summary diagrams (mean ± SEM) of data illustrated in A1 through C1. Spines undulating between SP- and
989   SP+ states were excluded and analyzed separately (c.f. Suppl. Fig. 5). (A1, A2) Initially SP+ spines surviving until
990   the end of the observation period (n = 51). Spines are sub-grouped based on the day SP is lost from the spine.
991   Note the reduction of spine head size after loss of SP. (B1, B2) Initially SP+ spines that are pruned and go through
992   a SP- state prior to pruning (n = 34). X = lost. Spines are sub-grouped based on the day the spine is pruned. (C1,
993   2) Initially SP+ spines that are lost directly (n = 2; 5.56% of SP+ spines), i.e. without going through a SP- state.
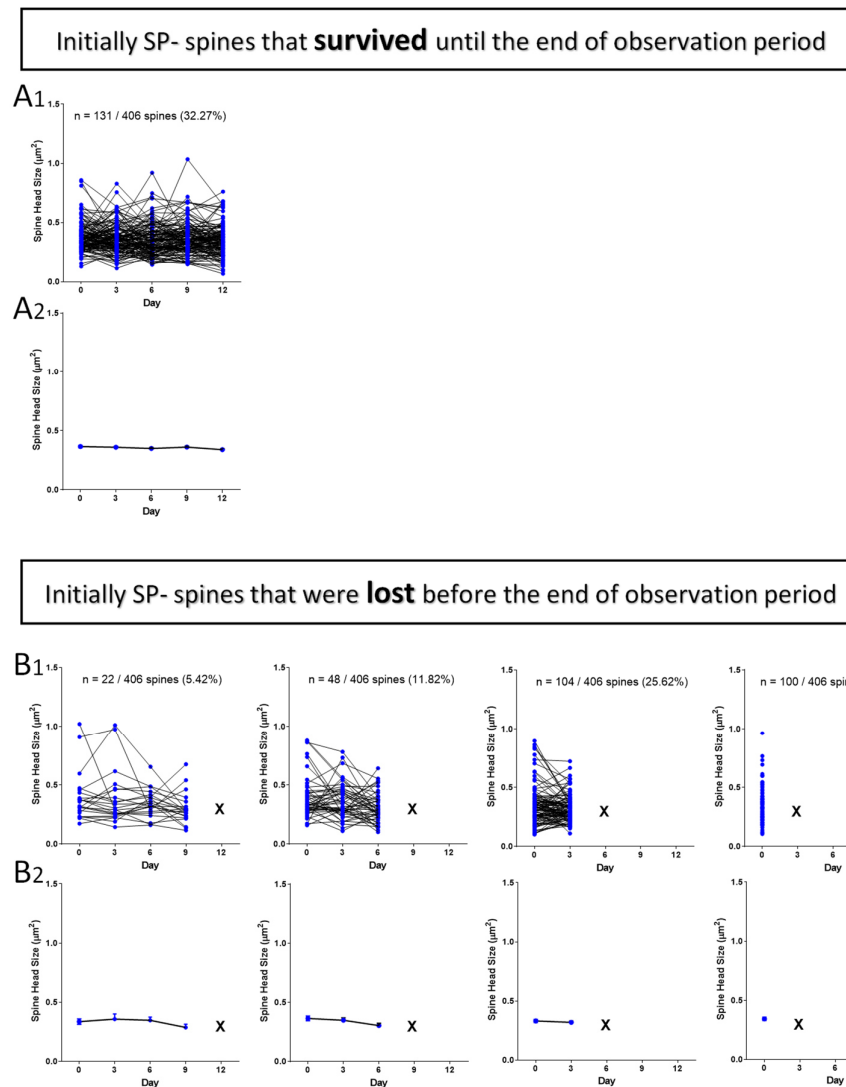994   These rare spines disappear sometime between imaging days 0 and 3.

Figure S4 related to Figure 7. Time-lapse 2-photon imaging data of individual SP- spines. SP- spines (SP- on day 0) are subdivided into two categories: (A) spines that survive until the end of the observation period (n = 131), (B) spines that are lost (n = 275). The fractions, percentages and SP-content (SP-, blue) of spines in the different sub-categories are shown. Upper panels (A1 and B1) show individual spines, lower panels (A2 and B2) show summary diagrams (mean ± SEM) of data shown in A1 and B1. Spines undulating between SP+ and SP- states are excluded and analyzed separately (c.f. Suppl. Fig. 5).
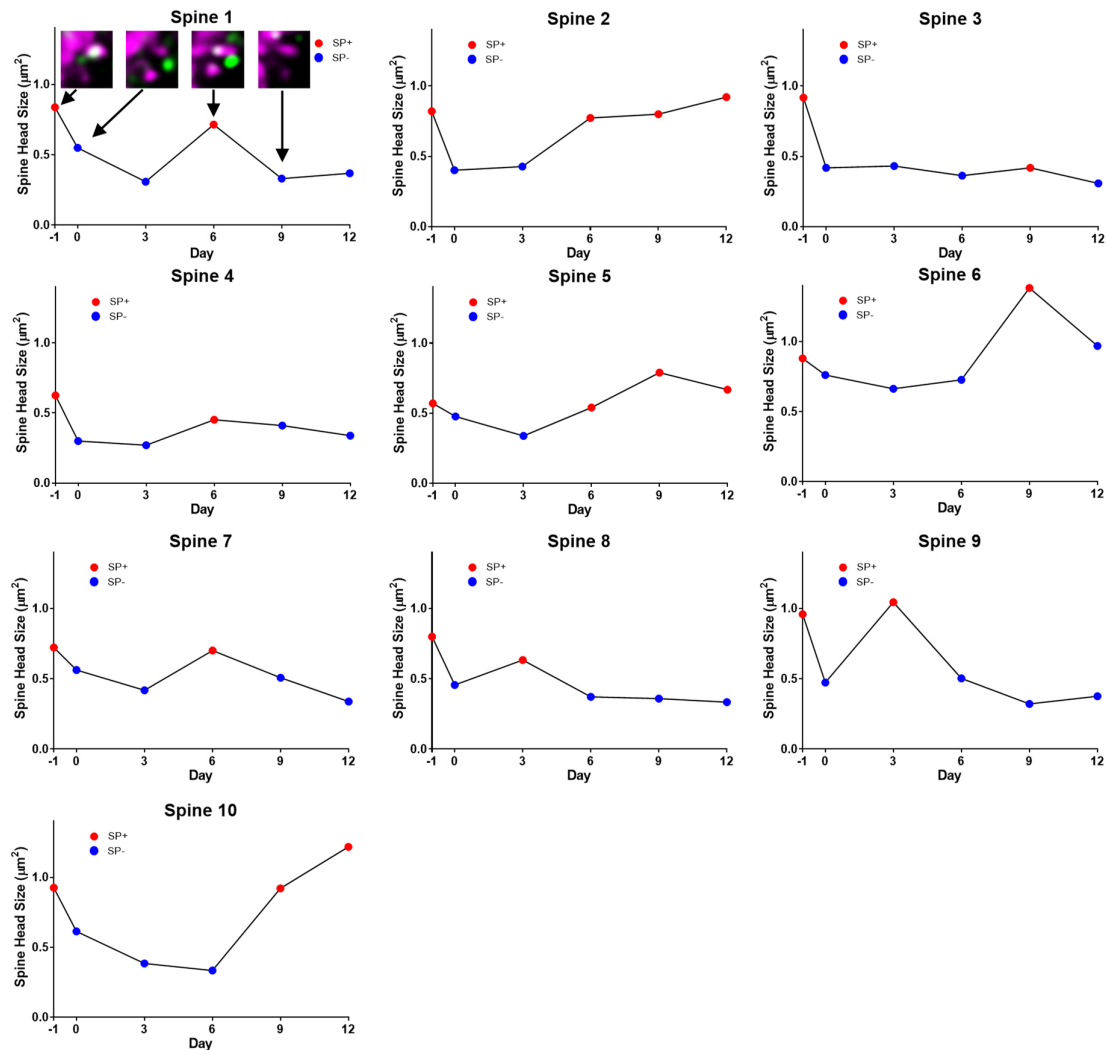
1002

Figure S5 related to Figure 7. Time-lapse 2-photon imaging data of individual spines undulating between SP+ and SP- states. Some SP+ spines loose SP and subsequently regain SP. This demonstrates that loss of SP from spines is not sufficient for spine pruning. Note corresponding changes in SP-content and in spine head size. The example of an undulating spine illustrated in Fig. 7I (lower part) is shown in this figure with all imaging time points (Spine 1).